Department of Precision and Microsystems Engineering

Design of actively controlled heat exchangers using topology optimization

Hari Mohanachandran

Report no : 2017.043
Coaches : Ir. M. van der Kolk, Dr. ir. D. Heck
Coaches : Eng. P. Smulders
Professor : Prof. dr. ir. A. van Keulen
Specialisation : Engineering mechanics
Type of report : Master thesis
Date : 27-09-2017

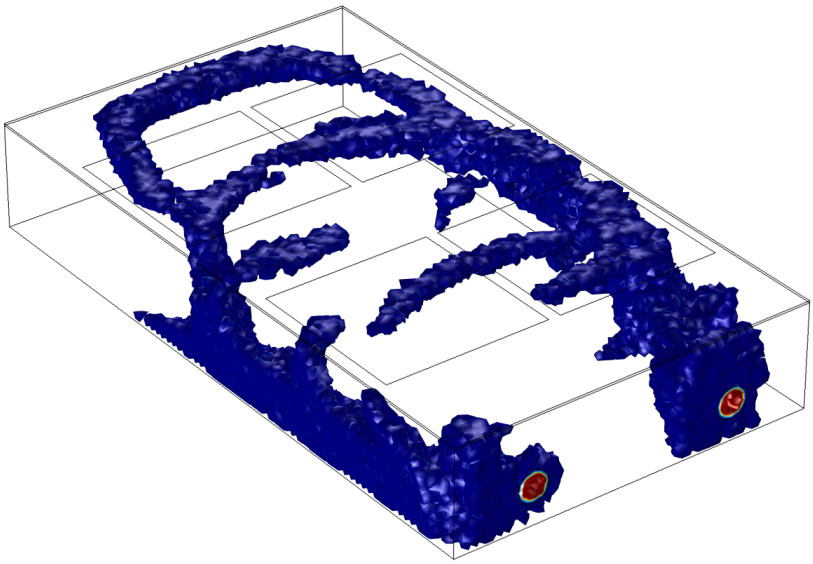

Design of actively controlled heat exchangers using topology optimization

Master thesis

by

Hari Mohanachandran

in partial fulfillment of the requirements for the degree of

Master of Science
in Mechanical Engineering

at the Delft University of Technology,
to be defended publicly on Tuesday September 27, 2017 at 13:45.

Student number:	4501152	
Thesis committee:	Prof. dr. ir. A. van Keulen,	TU Delft
	Dr. S. H. Hossein Nia Kani,	TU Delft
	Dr. R. Delfos,	TU Delft
	Ir. M. van der Kolk,	TU Delft
	Eng. P. Smulders,	Segula Technologies Nederlan B.V.

Abstract

An active fluid heat exchanger can be controlled effectively using Peltier elements to condition the temperature of the fluid flowing through the heat exchanger. The thermal resistance of the heat exchanger can be reduced to increase the speed of controlling the fluid's temperature. Topology optimization is used in this study to find the geometry of a heat exchanger with reduced thermal resistance.

The design of a heat exchanger using topology optimization requires the coupling of the fluid flow equations and the energy equation in a finite element model with a continuous design variable. The existing optimization models perform well when the goal of the optimization problem is to minimize viscous dissipation. A weighted sum multi-objective function is however necessary to optimize the thermal performance of a design, and the correct choice of weights to meet design specifications is difficult to arrive at.

The drawback in the existing model is that the conductivity distribution is defined as a function of the design variable of the optimization problem. This results in infeasible designs when the goal of the optimization problem is to minimize only thermal resistance, and this is demonstrated with several numerical examples along with a motivation for a new formulation.

A new formulation for conductivity distribution is proposed in this thesis. The new formulation defines the conductivity distribution in terms of the velocity field in the design domain. The new formulation is capable of significantly reducing the thermal resistance of the heat exchanger, and this is demonstrated with a numerical example. Finally, a 3d design case is implemented, the results of the optimization routine are post-processed and the performance of the baseline design from ASML is compared with the topology optimized design.

Acknowledgements

During an oral exam for a course on the stability of thin walled structures, I was stuck with a question. Fred van Keulen was the proffessor, and his advise was 'think about what is physically happening in the system'. I think that this is a very nice way of thinking, especially when we work in an abstract computational setting, and it is easy to lose sight of the goals we set initially.

I would like to thank Max van der Kolk for his support and encouragement throughout the project. He always asked me fundamental questions, which guided me in the right direction. In the early stages of the project I had some difficulty in coming up with a research question, and Dennis Heck's guidance was valuable in helping me get started. I would also like to thank Patrick Smulders for his guidance and feedback during the project.

Finally, I would like to thank my parents for imparting a critical attitude early on in me. I'm grateful for their support and love.

Contents

List of Figures

List of Tables

Nomenclature

Symbols

α	Brinkmann penalization parameter
$\alpha_{\max}$	maximum value of the Brinkmann penalization parameter
$\alpha_{\min}$	minimum value of the Brinkmann penalization parameter
ΔT_{lm}	logarithimic difference in temperature
Δ	difference operator
$\dot{m}$	mass flow rate
γ	design variable in the optimization problem
μ	coefficient of viscosity
$\nabla\cdot$	divergence operator
$\overline{h}$	average heat transfer coefficient
ϕ_α	function used to measure flow through porous regions
ϕ_{d}	viscous dissipation of energy
ϕ_{T}	function used in the objective to minimize viscous dissipation
ρ_{f}	density of fluid
σ	stress
τ	shear stress
A	area
C_p	specific heat capacity at constant pressure
d	diameter
f_{d}	dissipated power
f_{r}	recovered power
h_{c}	heat transfer coefficient at the cold plate of the Peltier element
h_{h}	heat transfer coefficient at the hot plate of the Peltier element
I	current
k	coefficient of conductivity

k_{Al}	conductivity of aluminum
k_{f}	conductivity of fluid
k_{s}	conductivity of solid
k_{water}	conductivity of water
L	channel length
P	penalization parameter
p	pressure
Pr	Prandtl number
Q	heat flux
q	interpolation parameter defining the steepness of the RAMP function
q_{conv}	convective heat flux
Q_{c}	heat flux at the cold plate of the Peltier element
Q_{gen}	heat generated per unit volume
Q_{h}	heat flux at the hot plate of the Peltier element
R	electrical resistance
R_{th}	thermal resistance
Re	Reynolds number
S	Seebeck coefficient
s	SIMP interpolation function
T	temperature
t	time
T_{m}	mean temperature
T_{int}	integral of the temperature at the outlet
T_{c}	cold plate temperature of the Peltier element
T_{h}	hot plate temperature of the Peltier element
T_{i}	average inlet temperature of the fluid
T_{o}	average outlet temperature of the fluid
V	potential difference
v	velocity
v_{max}	maximum channel velocity
Z	thermoelectric figure of merit of material
g	gravitational constant

Chapter 1

Introduction

The human body functions best when its temperature is between 36.5°C to 37.5°C. The rate of chemical reactions is a function of body temperature, and there are several control mechanisms to stabilize temperature. The hypothalamus is the temperature controller of the human body. It receives information from sensory organs and it sends signals to activate the control mechanisms. The body forms an active control system to function optimally even when the external environmental conditions are outside the optimal operating range.

Similarly, critical machine components require high temperature stability. These components are conditioned with the help of a temperature stabilized fluid for optimal performance. However, thermal variations enter the fluid through the environment. This degrades machine performance. Therefore, the fluid is sent to a heat exchanger to stabilize it. Since external heat sources can lead to an increase or decrease in fluid temperature, the heat exchanger requires either large damping or active control. An active control system is used for stabilization as this provides larger flexibitlity to achieve multiple temperature setpoints. A thermal actuator is used with a control system to stabilize the fluid temperature. The heat exchanger, thermal actuator and control system form an active control system hence referred to as an active heat exchanger.

Peltier elements are the thermo-electrical actuators used in the active heat exchanger. The amount of heat it pumps is current controlled. The use of Peltier elements as actuators has many advantages: they are robust, they have low performance degradation over time, they have a compact design and they have no moving parts. Therefore a Peltier element is used as the actuator to stabilize the fluid temperature. However a drawback of Peltier elements is their low energy efficiency when compared to other cooling technologies [3] like Stirling cycle refrigerators and vapor compression refrigerators.

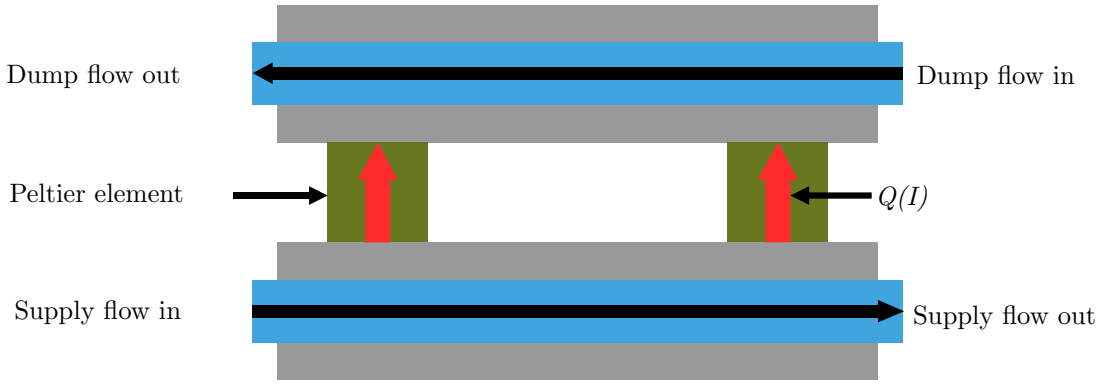

Figure 1.1: A fluid-fluid heat exchanger with a Peltier element working as a current controlled thermo-electric actuator.

Figure 1.1 shows the configuration of the active heat exchanger housing. The blue regions in the figure indicate fluid channels, the grey region is the metal, and the green regions indicate Peltier elements. The heat exchange between the fluid channels is indicated with a red arrow. The heat

exchanger has 2 separate fluid flow paths. One fluid is used to condition machine components, called the supply fluid. While the other fluid, called the dump fluid, removes or adds heat to the supply fluid to stabilize it. The supply and dump fluid channels have a metal housing surrounding them for efficient heat exchange via conduction. The actuator is placed between the supply and dump fluids to control the heat transferred between them. The fluid channels are placed in a counter flow configuration to improve the efficiency of heat exchange.

The active heat exchanger system is completed with a temperature sensor and controller as shown in Figure 1.2. T_{i} is the inlet temperature of the supply fluid with thermal variations. T_{o} is the stabilized outlet temperature of the supply fluid. The supply side is at the cold plate of the Peltier while the dump side is at the hot plate. The temperature setpoint of the supply side outlet is below its mean inlet temperature.

The outlet temperature of the fluid is measured by a sensor, and the controller computes the current required to provide the staibilizing heat flux. The interface temperature of the Peltier element and the supply side channel is T_{c}. The current defines the interface temperature, and therefore the heat flux.

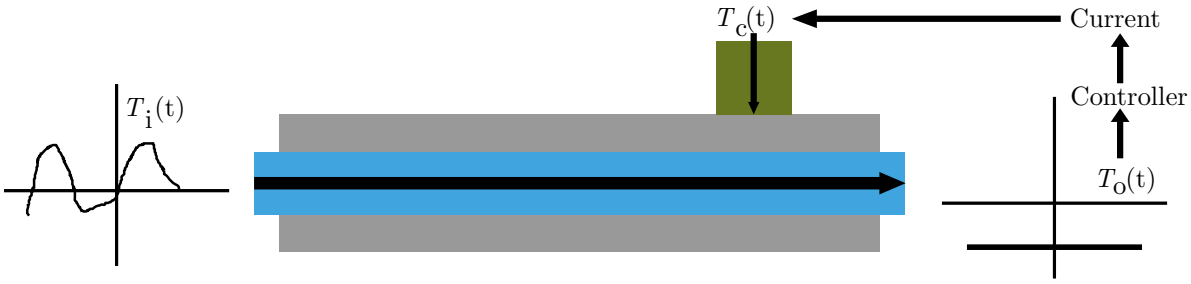

Figure 1.2: A control loop is used to stabilize temperature fluctuations in the fluid at the inlet of the heat exchanger with a controller and actuator.

1.1 Role of Peltier elements in the heat exchanger models

A Peltier element has two ceramic plates separated by a semiconductor p-n junction. The Peltier element operates on the Peltier effect. The Peltier effect produces a temperature difference across a conductor proportional to the potential difference across the conductor. The governing relationship between potential difference and temperature difference is expressed as

$$V = S\Delta T, \tag{1.1}$$

where S is the Seebeck coefficient, V the potential difference, and ΔT the difference between the hot and cold plate temperatures. Peltier elements use p-n junctions in their construction as they have a large Seebeck coefficient, and a material with a large Seebeck coefficient requires a smaller potential difference to produce a given temperature difference.

Figure 1.3 illustrates the heat transfer mechanism of the Peltier element. Q_{c} and Q_{h} are the heat transferred at the cold and hot plates of the Peltier element respectively. They are defined as

$$Q_{\mathrm{c}} = h_{\mathrm{c}} A(T_{\mathrm{h}} - T_{\mathrm{d}}), \tag{1.2}$$

$$Q_{\mathrm{h}} = h_{\mathrm{h}} A(T_{\mathrm{s}} - T_{\mathrm{c}}). \tag{1.3}$$

T_{h}, T_{c}, T_{s} and T_{d} are the temperatures of the hot plate, cold plate, supply fluid and dump fluid respectively. While h_{c} and h_{h} are the heat transfer coefficients at the cold and hot plates.

Heat transfer in the Peltier element is due to charge carriers in the p-n junction [4]. The majority charge carriers of the p junction are holes while the majority charge carriers of the n junction are electrons. The majority charge carriers transport heat as they move between the plates of the Peltier. In a steady state scenario each plate of the Peltier has a constant temperature that is

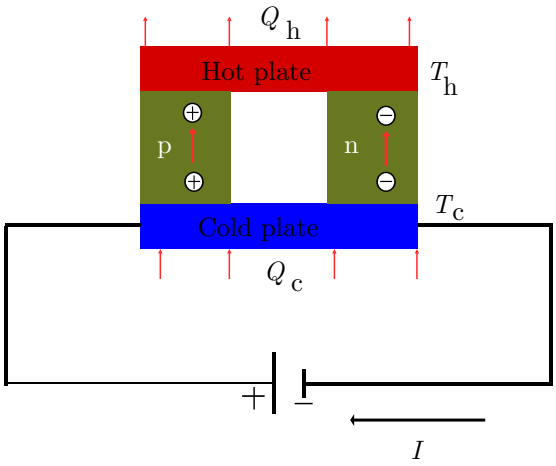

Figure 1.3: The Peltier element works as a heat pump with the majority charge carriers carrying heat when a potential difference exists between the plates of the element.

a function of current as well as the heat transfer coefficients at each of the plates. Appendix A describes the steady state Peltier model that defines the plate temperatures.

The heat transferred at each plate of the Peltier is a function of the supply and dump side fluid channel geometries as they define h_c and h_h. As the thermal performance of the heat exchangers improve the amount of heat transferred from the supply fluid to the dump fluid for a given ΔT is higher. This reduces the operating voltage for a given ΔT, and it improves the speed of controlling the fluid's temperature. The role of Peltier elements is reduced to a constant temperature boundary condition in the steady state model of the heat exchanger.

1.2 Scope of research

In general, existing heat exchangers at ASML have a large thermal resistance (see Appendix B for the definition of thermal resistance). This makes control of the heat exchanger challenging as the Peltier element is operated outside its optimal current range. The goal of this study is to implement a topology optimization model to find a 3d heat exchanger design with optimal thermal performance. The design also has a constraint on the viscous dissipation in the design. The design case for the heat exchanger is present at Segula Technologies Nederland B.V., while the heat exchangers are used in ASML.

Topology optimization is used to find the fluid channel geometry of the supply fluid to reduce the thermal resistance of the heat exchanger. The design of the dump side fluid channel is not considered in this study. The optimization uses a steady state model of the heat exchanger neglecting the transient damping behaviour in it. The thermal fluctuations in the supply fluid have large time constants, therfore the steady state performance of the heat exchanger is of primary importance.

Additionally a low Reynolds number model ($Re = 3.3$ in the 2d models used and a Stokes flow model is used in the 3d case) is used. This is to avoid convergence issues with the fluid flow model, and to avoid the complex flow patterns found in high Reynolds number flows. The focus of this study is to develop the optimization model of the heat exchanger.

Methods present in literature are initially implemented in this study to optimize the heat exchanger design. However certain limitations are encountered when the goal of the optimization problem is to minimize thermal resistance. Therefore a new optimization model is presented to overcome the limitations encountered in finding designs that have reduced thermal resistance.

1.3 Outline

An outline of the chapters in this thesis is presented to give the reader an idea about the contents of proceeding chapters. This is done to provide more clarity about modeling choices taken in earlier chapters.

Chapter 2 introduces the fluid flow and heat transfer models. This is followed by an introduction to optimization methods. The model of the heat exchanger is augmented with additinal parameters to enable topology optimization with continuous design variables. Sufficient examples from literature are reviewed to illustrate the augmented model.

Chapter 3 defines a 2d design domain and presents the design problem of a convective heat transfer system. The conductivity of the full design domain is defined using the conductivity of the fluid in this chapter. Motivations for this approach are provided in Chapter 2.

Chapter 4 studies the conductivity interpolation models reviewed in literature using the 2d design domain defined in Chapter 3. The conductivity interpolation model allows the definition of fluid and solid conductivities. The erosion of the optimization model in specific situations is illustrated. The motivation to investigate a new conductivity interpolation model is given.

Chapter 5 defines a new conductivity interpolation model along with a numerical example to validate it. Chapter 6 implements the new interpolation model to the 3d design case at ASML, and a final design is presented. The conclusions and scope for future research are presented in Chapter 7.

Chapter 2

Literature review

The design of a heat exhanger using an optimization method requires a model for fluid dynamics and heat transfer. The first section of this chapter describes the relevant models used in this study. This is followed by an introduction to topology optimization. Methods to combine the models and to introduce a continuous design variable to optimize the heat exchanger are then reviewed.

2.1 Fluid dynamics and heat transfer

2.1.1 Fluid dynamics

A laminar viscous flow model is used to study the behaviour of the fluid in the heat exchanger. In a viscous flow model the fluid velocity is zero at the surface of a solid, and the velocity increases away from the solid. The fast moving layers of a fluid try to speed up slower layers and vice versa. This is because of collisions between the molecules of the fluid, and it leads to the viscous dissipation of energy. Viscous dissipation is compensated by a pump in an internal flow heat exchanger.

In external flows viscous forces are also known as skin friction drag forces. The design of the wings of an airplane for instance are designed to minimize these drag forces to reduce the amount of work done by the engines. Similarly, heat exchangers are also designed to minimize the work done by the pump, while maintaining large heat transfer coefficients.

Conservation of mass and momentum equations

The velocity and pressure fields in the domain are found by solving the continuity and momentum equations. The continuity equation for a fluid is

$$\frac{\partial \rho_\mathrm{f}}{\partial t} + \frac{\partial \rho_\mathrm{f} v_i}{\partial x_i} = 0, \tag{2.1}$$

where ρ_f is the density of the fluid and t is time. The symbol v denotes velocity and the subscript i identifies the component. Similarly, x_i is a component of the spatial field. Additionally, when the density of the fluid is assumed to be constant the continuity equation reduces to

$$\frac{\partial \rho_\mathrm{f}}{\partial t} + \rho_\mathrm{f} \frac{\partial v_i}{\partial x_i} = 0. \tag{2.2}$$

A steady state model of the heat exchanger is studied in this thesis. Therefore the derivatives of time are neglected. The steady state continuity equation for an incompressible fluid reduces to

$$\nabla \cdot \boldsymbol{v} = 0 \tag{2.3}$$

in vector notation. Where $\nabla\cdot$ is the divergence operator. A bold symbol is used to indicate vectors. The momentum equation in the scalar form reads

$$\rho_{\mathrm{f}}\frac{Dv_i}{Dt} = -\rho_{\mathrm{f}}\mathrm{g}_i + \frac{\partial\sigma_{ij}}{\partial x_j}, \tag{2.4}$$

where D is the total derivative, g the gravitational constant and σ_{ij} are the components of the stress tensor. In the remainder of this work body forces ($\rho_{\mathrm{f}}\mathrm{g}_i$) are neglected. Expanding the stress tensor and the total derivative the momentum equation becomes

$$\rho_{\mathrm{f}}\frac{\partial v_i}{\partial t} + \rho_{\mathrm{f}}\left(v_j\frac{\partial}{\partial x_j}\right)v_i = -\frac{\partial p}{\partial x_i} + \frac{\partial\tau_{ij}}{\partial x_j}, \tag{2.5}$$

where p is the pressure field and τ_{ij} are the components of the shear stress tensor. The steady state assumption is used, and the material model linking the velocity field and shear stresses of a Newtonian fluid are used to arrive at

$$\rho_{\mathrm{f}}\left(v_j\frac{\partial}{\partial x_j}\right)v_i = -\frac{\partial p}{\partial x_i} + \mu\frac{\partial^2 v_i}{\partial x_j\partial x_j}, \tag{2.6}$$

which is further rewritten in vector notation as

$$\rho_{\mathrm{f}}(\boldsymbol{v}\cdot\nabla)\boldsymbol{v} = -\nabla p + \mu\nabla^2\boldsymbol{v}. \tag{2.7}$$

Where μ is the coefficient of viscosity of a fluid. The first term is the convective acceleration force, while the second and third term are the pressure and shear forces acting on a fluid element.

The momentum equation is scaled in the following manner to make it non-dimensional: $\boldsymbol{x}^* = \frac{\boldsymbol{x}}{\mathrm{L}}$, $\boldsymbol{v}^* = \frac{\boldsymbol{v}}{U}$, $p^* = \frac{p-p_\infty}{\mu U_i/L}$ and ∇^* is the divergence operator with the scaled spatial field $\boldsymbol{x}^*$, where L, U are the charecteristic length and velocity. p_∞ is the free stream pressure. The scaled momentum equation becomes

$$Re(\boldsymbol{v}^*\cdot\nabla^*)\boldsymbol{v}^* = -\nabla^* p^* + \nabla^{*2}\boldsymbol{v}^*. \tag{2.8}$$

The first term in the above equation scales with the Reynolds number. Low Reynolds number flows have a low pressure drop due to convective acceleration. Further, a Stokes flow model neglects the inertial terms due to convective acceleration to reduce the momentum balance between the pressure gradients and the viscous forces. The Stokes flow momentum equation is

$$\nabla p = \mu\nabla^2\boldsymbol{v}. \tag{2.9}$$

2.1.2 Heat transfer

The temperature field in the fluid is determined using the convection diffusion equation. It is solved using the velocity field determined from the mass and momentum conservation equations. A one way coupling is used as the material properties of the fluid are assumed to be independent of temperature. The convection diffusion equation for an incompressible fluid is

$$\rho_{\mathrm{f}}C_p\frac{\partial T}{\partial t} + \rho_{\mathrm{f}}C_p\boldsymbol{v}\cdot\nabla T + \nabla.\boldsymbol{Q} = Q_{\mathrm{gen}} + \phi_{\mathrm{d}}, \tag{2.10}$$

where C_p is the specific heat capacity of the fluid at constant pressure, T denotes temperature and Q_{gen} is a heat source term. The dissipation term ϕ_{d} is neglected in the energy equation for low Reynolds number models. The energy equation reduces to

$$\rho_{\mathrm{f}}C_{\mathrm{p}}\boldsymbol{v}\cdot\nabla T + \nabla\cdot\boldsymbol{Q} = Q_{\mathrm{gen}} \tag{2.11}$$

in a steady state scenario. The first term is the convective flux and $\boldsymbol{Q}$ is the conductive flux . The conductive flux is expanded as

$$\boldsymbol{Q} = -k\nabla T, \tag{2.12}$$

where k is the coefficient of conductivity. Solid regions have only conductive heat transfer as the velocity field goes to zero. The energy balance in solid regions reduces to

$$\nabla \cdot \boldsymbol{Q} = 0. \tag{2.13}$$

The reader is refered to Frank M. White's Viscous fluid flow [5] for an in depth study of viscous flows.

2.2 Optimization

An optimization problem is defined as the task of finding the best possible solution in $\mathbb{R}^n$ from a set of suitable candidates. The mathematical form of an optimization problem is [6]

$$\begin{aligned} &\text{minimize} && f_0(\boldsymbol{x}) \\ &\text{subject to} && f_i(\boldsymbol{x}) \leq \boldsymbol{b}_i, \quad i=1,...,m \\ &&& h_j(\boldsymbol{x}) = 0, \quad j=1,...,n \end{aligned}$$

Where $\mathrm{f}_0 : \mathbb{R}^n \to \mathbb{R}$ is the objective function, $f_i : \mathbb{R}^n \to \mathbb{R}$ the inequality constraints with bounds b_i, and $h_j : \mathbb{R}^n \to \mathbb{R}$ the equality constraints. The objective function is interpreted as the cost assigned to a design $\boldsymbol{x}$, and the best design ($\hat{\boldsymbol{x}}^*$) has the lowest cost within the feasible set.

The objective functions used in heat exchanger design problems are usually the financial cost of the heat exchanger, a measure of thermal performance and a measure of viscous dissipation. While the design variables of the optimization problem depend on the freedom provided to the optimizer. The design variables in a mechanics problem are classified based on size, shape and topology optimization [7].

A size optimization problem has a predefined geometry and the size of different components are optimized. Heat exchanger design problems generally optimize the dimension of tubes or the spacing between tubes. Patel et al. [8] minimize the manufacturing cost of a shell and tube heat exchanger by optimizing the shell diameters and the baffle spacing in the design. While Foli et al. [9] use a multi-objective function to minimize the the pressure drop and maximize heat transfer in a microchannel heat exchanger. The design variables of the optimization problem are the height and length of the channels. They use a weighted sum approach on the objective function to find the pareto front of the optimization problem.

Shape optimization problems also have a pre-defined topology, however the optimizer has the additional freedom to change the shape as well as the size of a structure. The optimizer has the freedom to change a circle to a square in a shape optimization problem, while optimizing the area of the design as well. Hilbert et al. [10] use shape optimization to design the blades of a heat exchanger using a multi-objective function that minimizes the weighted sum of the pressure drop and temperature drop of a fluid in the heat exchanger.

A topology optimization problem aims to optimize the material distribution within a design domain. The connectivity of structures is not defined apriori, and it evolves during the optimization process. It is a powerful technique to generate complex designs. Therefore, topology optimization is used in this study to design heat exchangers.

A topology optimization problem assigns a material density to each element of the finite element model of the problem; this results in a large number of design variables. Therefore, a gradient based approach is used to iterate towards an optimal design to reduce computational complexity. The next section reviews methods to combine the fluid flow model, the heat transfer model and formulate a gradient based optimization problem.

2.3 Topology optimization of a convective heat transfer system

2.3.1 Optimization in fluid flow systems

Borrvall and Petersson [1] introduced the Darcy equation for flow through porous media to formulate a fluid flow topology optimization problem. The Darcy equation is formulated with an additional parameter in the momentum equation

$$\rho_{\mathrm{f}}(\boldsymbol{v}\cdot\nabla)\boldsymbol{v} = -\nabla p + \mu\nabla^2\boldsymbol{v} - \alpha\boldsymbol{v}, \tag{2.14}$$

where (α) is the additional parameter that penalizes the velocity field. Solid regions in the design domain have maximum penalization ($\alpha_{\max}$) to approximate the no-slip condition, while fluid regions have minimum penalization ($\alpha_{\min}$) to recover the original momentum equation. Additionally, flow through porous regions lead to an increase in pressure drop as both α and velocity is large when there is porous flow.

A continuous design variable is used to transition from a solid to a fluid region. The design variable of the topology optimization problem is defined as

$$\gamma = 0 : \text{solid} \tag{2.15}$$

$$\gamma = 1 : \text{fluid} \tag{2.16}$$

and the bounds of the design variable are

$$0 \leq \gamma \leq 1. \tag{2.17}$$

The interpolation function Borrvall and Petersson used to transition from maximum to minimum penalization is

$$\alpha = \alpha_{\max} + (\alpha_{\min} - \alpha_{\max})\gamma(\frac{1+q}{\gamma+q}), \tag{2.18}$$

where q is a parameter that defines the steepness of the function. Figure 2.1 shows the porous flow penalization parameter as a function of the design variable for different q. As the magnitude of q is increased intermediate values of the design variable are increasingly penalized. A continuation strategy is implemented in this study where q is incremented after a given number of iterations. This is done as small values of q help avoid local optima, while large values of it help arrive at black and white designs.

Borrvall and Petersson designed a pipe to minimize the viscous dissipation in the design using the above formulation. The design domain they used is shown in Figure 2.2. Figure 2.3 shows the topology optimized designs they found for a fine and coarse mesh using a Stokes flow model. The optimized designs are independent of the mesh size used for the given problem. The design minimizes pumping power by reducing the length from entry to exit and by maximizing the area of the pipe (a volume constraint is present on the fluid regions). The objective function they used is

$$\phi_{\mathrm{T}} = \int_{\omega}[\mu\frac{\partial v_i}{\partial x_j}\frac{\partial v_i}{\partial x_j} + \alpha v_i v_i]d\mathrm{x}, \tag{2.19}$$

where the functions in the integral are separated and defined as

$$\phi_{\mathrm{d}} = \int_{\omega}[\mu\frac{\partial v_i}{\partial x_j}\frac{\partial v_i}{\partial x_j}]d\mathrm{x}, \tag{2.20}$$

and

$$\phi_{\alpha} = \int_{\omega}[\alpha v_i v_i]d\mathrm{x}. \tag{2.21}$$

ϕ_{d} is the viscous dissipation and ϕ_{α} is the cost assigned to penalize flow through porous regions respectively.

Gersborg-Hansen et al. [11] extended the formulation to non-linear flows, and they studied the influence of the momentum terms on viscous dissipation. Similarly Kreissl [12] extended the use of the above objective in a transient scenario to minimize viscous dissipation in systems.

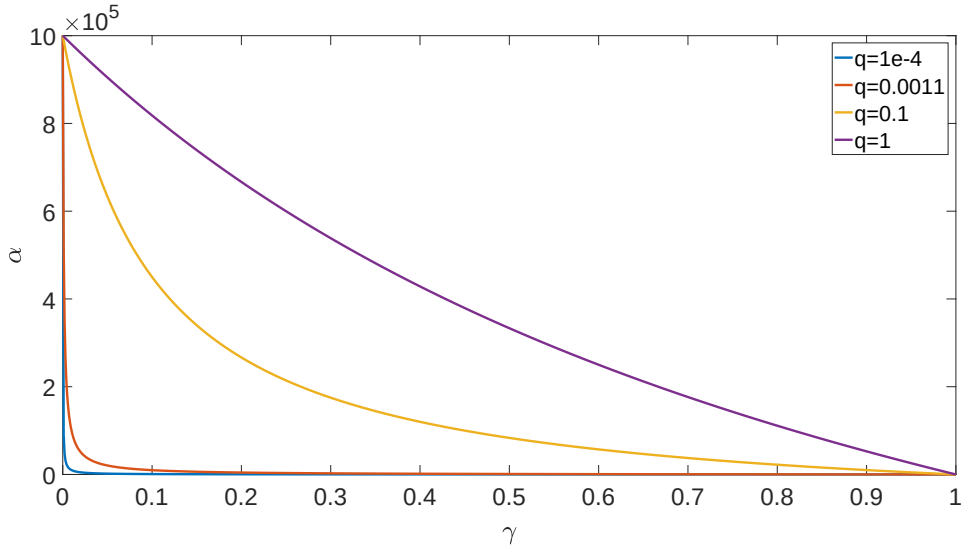

Figure 2.1: Interpolation of the penalization parameter α for different q. The penalization at intermediate densities is defined by how large q is.

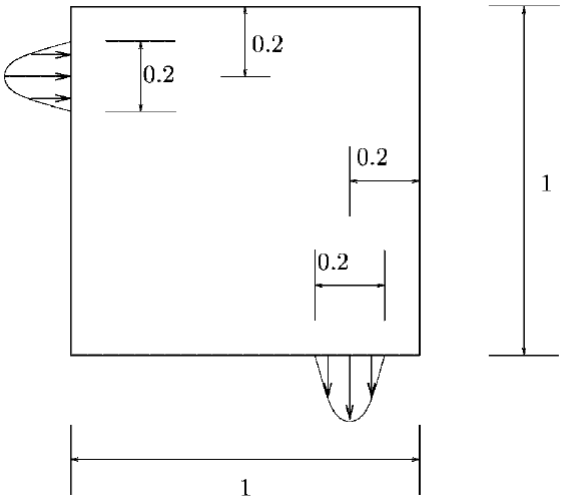

Figure 2.2: Design domain used to find the geometry of a pipe that minimizes viscous dissipation [1].

2.3.2 Optimization in heat transfer systems

Gersborg-Hansen et al. [13] designed a heat conduction system to minimize the temperature gradients in a domain. The amount of high conductivity material is limited by a volume constraint in the optimization problem. They used the solid isotropic material with penalization rule (SIMP) to allocate conductivity within the domain. Conductivity is a function of the design variable through the SIMP function $\boldsymbol{s}$ as

$$\boldsymbol{k} = \boldsymbol{s}(\boldsymbol{\gamma}), \qquad s_{\mathrm{i}}(\gamma_i) = \gamma_{\min} + (1 - \gamma_{\min}){\gamma_{\mathrm{i}}}^P, \tag{2.22}$$

where $\gamma_{\min}$ is the minimum value of the design variable allowed and P is a penalization factor that defines the conductivity for intermediate values of the design variable. They found fin like metal structures that spread heat throughout the domain with a constant heat load to minimize temperature gradients. Similarly Marck et al. [14] use the SIMP formulation to minimize the average and variance of the temperature distribution within the design domain using a multi-objective function. The topology optimized designs have similar fin like structures. While Gao et

Figure 2.3: Optimized pipe geometries for a coarse and fine mesh that minimize viscous dissipation [1] using a Stokes flow model.

al. [15] extended the study to design dependent heat loads.

The energy equation of a convective heat transfer system (2.11) has a coupling to the velocity field. The velocity field is solved using the fluid flow model illustrated by Borrvall and Petersson to define solid and fluid areas in the domain. Since a steady state analysis is performed the only thermal material property of interest is conductivity. Marck et al. [16] used the ramp interpolation function to define conductivity. It is defined as

$$k = k_{\mathrm{s}} + (k_{\mathrm{f}} - k_{\mathrm{s}})\gamma(\frac{1+q}{\gamma+q}), \tag{2.23}$$

where k is the conductivity assigned to an element, k_{f} is the conductivity of the fluid, k_{s} the conductivity of the solid and q is the interpolation parameter defined in Equation 2.18. Koga [17] uses the SIMP interpolation model given in Equation 2.22 to define conductivity in the domain of a convective heat transfer system. Dede [18], Kyngjun Lee [19] and Pietropaoli et al. [2] use similar material models with conductivity defined as a function of the design variable.

A weighted multi-objective function with one function minimizing pumping power while the other maximizing thermal performance is used in the above studies. The multi-objective function used by Marck is

$$f = -wf_{\mathrm{r}} + (1-w)f_{\mathrm{d}} \tag{2.24}$$

The thermal objective is defined as

$$f_{\mathrm{r}} = \int [\boldsymbol{n} \cdot \boldsymbol{v}\rho C_p T]dL, \tag{2.25}$$

where f_{r} is the thermal power recovered, and the integral is evaluated at the outlet. While the viscous dissipation objective is defined as

$$f_{\mathrm{d}} = \int [\boldsymbol{n} \cdot \boldsymbol{v}(p + \frac{1}{2}\rho|\boldsymbol{v}|^2)]dL, \tag{2.26}$$

where f_{d} is total viscous power dissipated as the fluid reaches the outlet.

Dede and Kyungjun Lee have the thermal objective of minimizing the temperature gradients within the domain, which is the objective function used in the heat conduction systems reviewed earlier. While Marck et al. and Pietropaoli et al. maximize heat exchange between the fluid and the boundaries of the domain.

Pietrapaoli et al. additionally use a frozen turbulence approach with a $k-\epsilon$ model in their study. They use a box with the top and bottom plates of the box acting as constant temperature hot plates in the design domain. Figure 2.4 shows the topology optimized designs they found with different weights used in the multi-objective function. As the weight on the thermal objective is increased the fluid flow splits to the hot plates at the top and bottom to increase heat transfer.

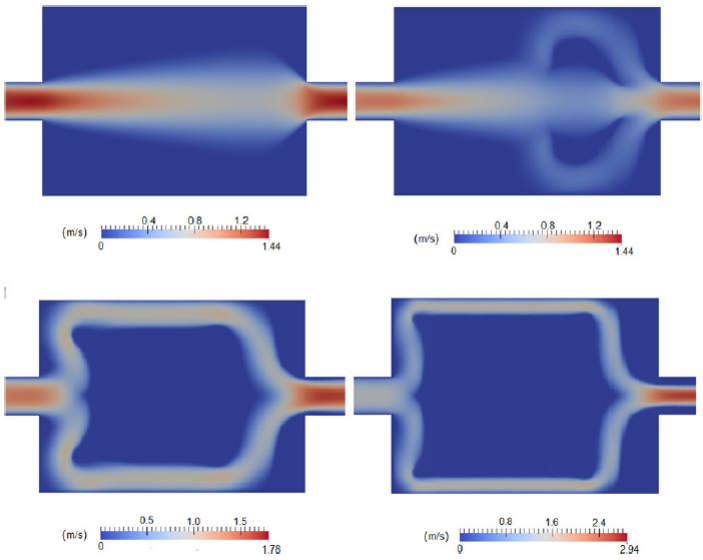

Figure 2.4: Topology optimized ducts found for different scaling of weights in the objective functions [2]. The designs from left to right and top to bottom have an increased weight on the thermal objective. The ducts split and become narrower to increase the heat transfer coefficient at the top and bottom hot plates.

The ducts in the last design case become narrower to increase the heat transfer coefficient of the fluid channel to improve thermal performance further. The influence of channel geometry on heat transfer coefficient is reviewed in Appendix C.

Discussion

A weighted sum apporach is used in the studies reviewed on the design of convective heat transfer systems. The weights on the thermal and pumping power objective are tuned to find the pareto front of the optimization problem. However Kyungjun Lee noticed that the optimization problem erodes when only the thermal objective is used. The optimizer finds a solution that has porous flow through highly conductive solid regions to improve the thermal objective. The porous flow solution is a result of the misuse of the conductivity model. Therefore, Chapter 3 studies a convective heat transfer system without the conductivity interpolation model. A constant conductivity (k_f) is defined throughout the domain to initially study the convective heat transfer model.

Chapter 3

Topology optimization of a convective cooling system with uniform conductivity in design domain

This chapter defines a 2d optimization problem, and the results of the optimization problem are compared to a reference design. The goal of the optimization problem is to find a design that has a lower thermal resistance than the reference design, while limiting the viscous dissipation of the design below that of the reference design. A multi-objective function is defined, and different combinations of weights are investigated to arrive at a design that has the optimal trade-off between thermal resistance and viscous dissipation.

All simulations in this chapter use the conductivity of the fluid throughout the design domain. Therefore, regions with zero flow velocities also have the conductivity of the fluid. This formulation is used to study the optimization model for the single objective case of minimizing the outlet temperature of the fluid.

The heat transfer mechanism of the reference design is initially studied, followed by the definition of the multi-objective optimization problem. The thermal resistance and viscous dissipation of the optimized designs and reference design are then compared. The topology optimized designs are converted to black and white designs by post-processing to validate the performance of the design using a matching mesh and the fluid flow model.

The 2d design domain of the heat exchanger (see Figure 3.1) has a hot fluid entering with an inlet temperature T_{i}. Two cold plates are present at the top and the bottom of the domain at a temperature T_{c} for heat exchange. The cold plates represent the Peltier elements in a steady state scenario.

Table 3.1: Dimensions of the 2d design domain and parameters defining the boundary conditions of the domain.

Parameter	Magnitude
L	140 mm
H	140 mm
d	8 mm
T_{i}	330 K
T_{c}	275 K
Inlet Reynolds number	3.333

The dimensions of the design domain and parameters defining the boundary conditions of the domain are in Table 3.1. A square and symmetric design domain is chosen, while the dimensions

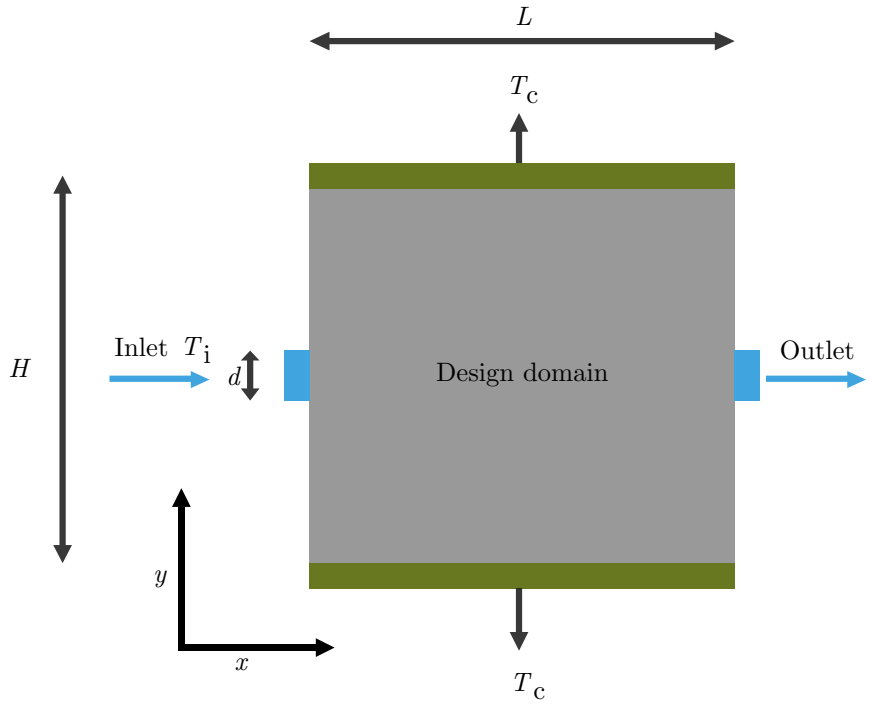

Figure 3.1: Domain used for the topology optimization of the 2d design problem.

of the square are chosen close to the dimensions of the 3d design case of Chapter 6. The Reynolds number of the design case is chosen close to 1, and the penalization parameter $\alpha_{\max}$ is selected as 1e6 from the study performed by Lee [19]. The material properties of water are in Table 3.2, and they are assumed to be independent of temperature.

Table 3.2: Material properties of water used in the optimization model.

Property	Magnitude
μ	1e-3 N-s/m^2
ρ	1000 kg/m^3
k_{water}	0.6 W/m-K
C_p	4182 J/Kg-K

3.1 Reference design to the optimization problem

Figure 3.2 shows the reference design to the optimization problem. It has rectangular fluid channels placed against the top and bottom cold plates for heat exchange. The channel thickness t is chosen as 10 mm. The average outlet temperature and viscous dissipation of the design are found using both the porous flow model and the fluid flow model to compare the performance of both models.

3.1.1 Influence of leakage in the porous flow model

Figure 3.3 shows the pressure field within the design domain found using the porous flow model. Leakage through the porous solid regions are present as there are pressure gradients within this region. Table 3.3 has the mass flow rate through each channel as well as the amount of leakage.

Table 3.4 compares the average outlet temperature and viscous dissipation of the porous flow and fluid flow models. The outlet temperature found using the porous flow model is higher, since the amount of fluid available at the cold plates is lower due to leakage. The leaked fluid also has a shorter distance to the outlet via the porous solid hence the viscous dissipation found using the porous flow model is lower. Inspite of the differences, the results found using both models are

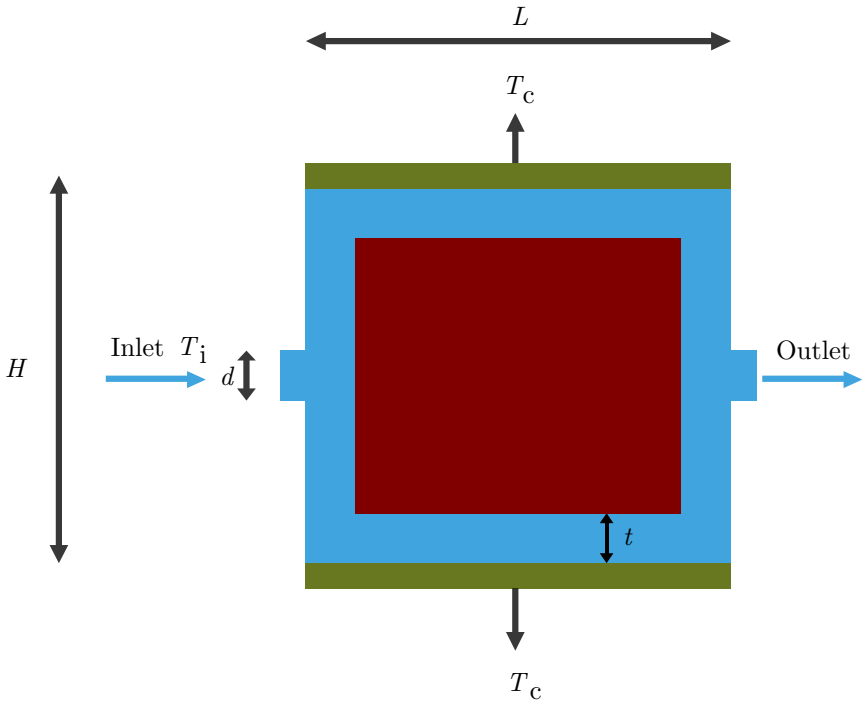

Figure 3.2: Reference design to the optimization problem has rectangular fluid channels placed along the cold plates. The fluid regions are shown in blue while the solid regions are shown in brown.

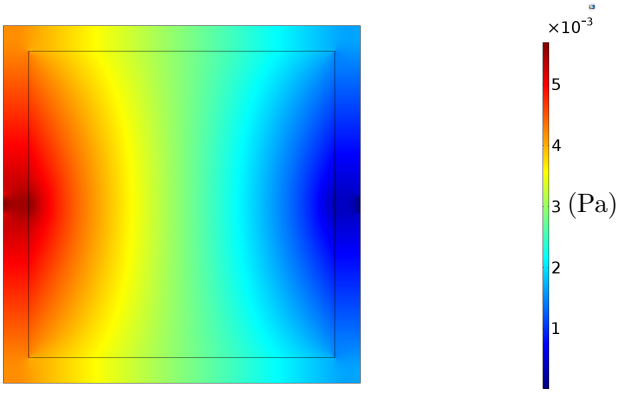

Figure 3.3: Pressure field in the reference design found using the porous flow model. There is a pressure gradient in the solid region as well indicating porous flow.

nearly identical for the reference design. Therefore, the porous flow model is used to approximate the fluid flow model for optimizing the design.

3.1.2 Heat transfer in the design

The streamline plot of the fluid is initially shown in all designs to see the path taken by the fluid in the domain. Regions with large convective transport are then identified using the convective product in the flow direction ($v_i T$), and the heat flux within the domain is additionally shown to identify the main modes of heat transfer at different locations of the domain.

In the reference design, the hot fluid at the inlet is directed towards the cold plates at the top and bottom via vertical channels. Next, the fluid flows along the cold plates and then to the outlet through vertical channels. Figure 3.4 shows the path taken by the fluid with the streamline plot found using the porous flow model. Figure 3.5 shows the temperature profile in the domain. The

Table 3.3: Mass flow distribution of fluid in the reference design to determine the amount of leakage through the porous solid.

Fluid channel	% mass flow
Top channel	49.87%
Bottom channel	49.87%
Leakage	0.26%

Table 3.4: Comparison of average outlet temperature and viscous dissipation between the porous flow model and the fluid flow model for the 2d reference design.

Parameter	ϕ_{d} (W)	T_{o} (K)
Fluid flow model	1.8658e-8	279.84
Porous flow model	1.8611e-8	279.87

fluid loses heat via convection to the cold plates. The convective flux is seen in regions with a large temperature gradient. These regions are highlighted in the figure. The temperature gradient within the solid region is due to a conductive heat flux.

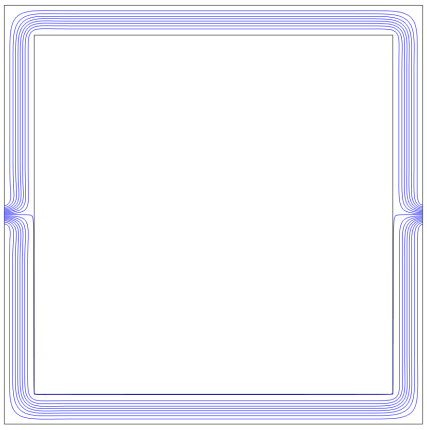

Figure 3.4: Streamline plot of fluid flow in the reference design found using the porous flow model.

Convective heat transfer is also present at the vertical walls at the inlet and outlet. The convective flux is seen from the heat flux plot of Figure 3.6. The heat flux in the horizontal direction is due to convective heat transfer at the vertical walls (the highlighted regions show the temperature gradient due to convective heat transfer).

At the corner, the fluid flow direction changes and it accelerates in the x-direction. The heat transfer mechanism switches from conduction to convection as the velocity field is zero at the corner. This results in a positive temperature gradient in the flow direction initially. The highlighted red regions in Figure 3.7 are a result of the switch in heat transfer mechanism. After the switch, heat is transferred via convection to the cold plates. This is seen as a negative temperature gradient in the convective product (uT_x) in the flow direction.

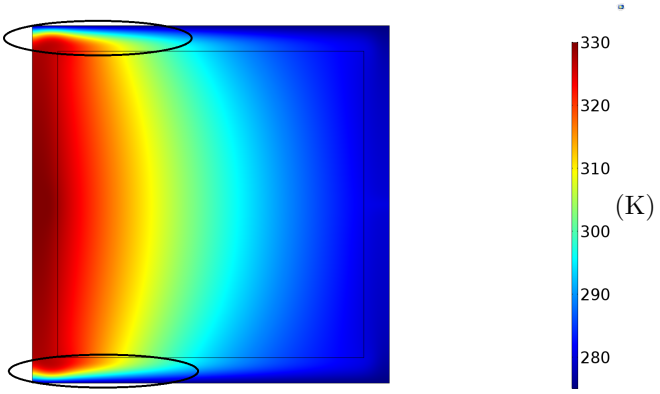

Figure 3.5: Temperature profile in the 2d reference design. The highlighted regions show the large temperature gradients due to convective heat transfer.

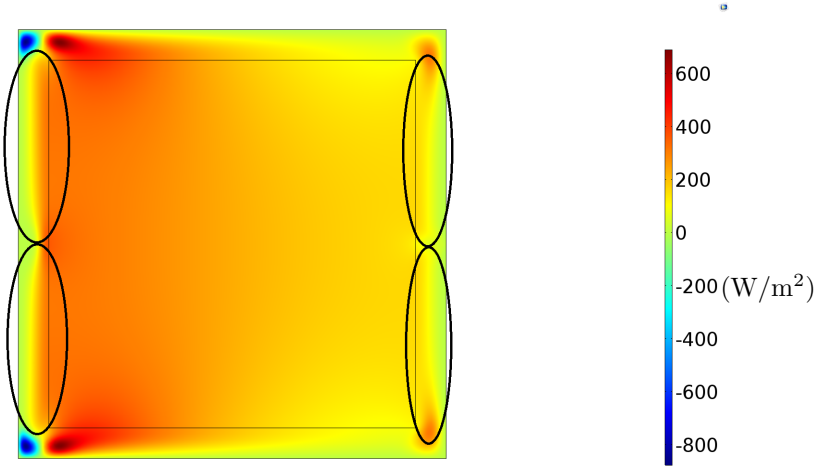

Figure 3.6: Heat flux in the horizontal direction is used to show convective heat transfer at the vertical walls.

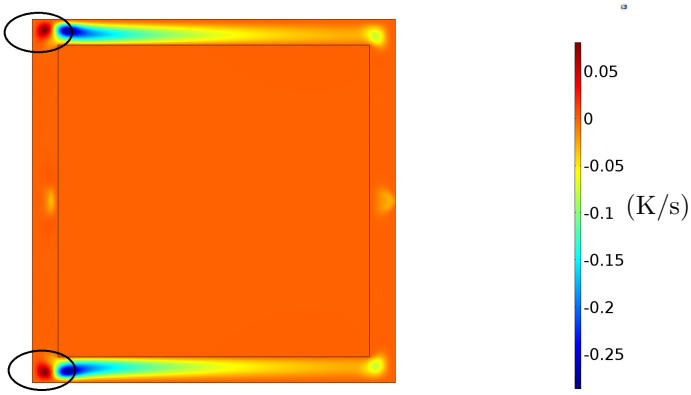

Figure 3.7: Convective product in the horizontal direction (uT_x) shows convective heat transfer in the fluid channels at the cold walls.

The heat flux and convective product plots shown earlier are a function of the temperature difference between the fluid and solid regions and the local heat transfer coefficient. Heat fluxes in the domain diminish towards the outlet as the temperature difference between the plates and the fluid become small. The heat transfer coefficient is a measure of thermal performance independent

of the temperature difference between the cold plate and the fluid. Therefore it is used to study the impact of the channel geometry on the outlet temperature, while the heat flux and convective products identify the dominant mode of heat transfer at a given location. Figure 3.8 shows the heat transfer coefficient of the reference design only at the top plate, since the design is symmetric.

The heat transfer coefficient is initially non-zero because of conductive heat transfer when the fluid velocity is zero. It then increases to a maxima; next it decreases to a constant value until the fluid changes direction towards the outlet. The temperature profile of the fluid is nearly uniform at the first corner, and this causes the heat transfer coefficient to be have a maxima close to the corner. This is similar to the heat transfer behaviour seen at the thermal entrance region. Additionally, the oscillations in the heat transfer coefficient are a result of the coarse mesh used in the model.

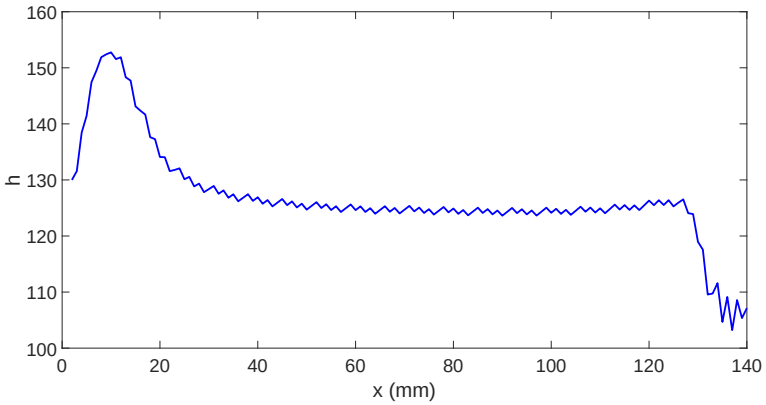

Figure 3.8: Heat transfer coefficient at the top wall of the 2d reference design. It is used as the measure of heat transfer as it is independent of temperature in the given problem.

3.2 Topology optimization of the 2d model

The optimization problem is solved using the GCMMA algorithm introduced by Svanberg [20] as it is the algorithm most commonly used in topology optimization problems. Moreover the Helmholtz partial differential equation filter [21] is implemented with a filter radius of 1 mm as it improves the performance of the optimization algorithm. The direct model as well as optimization is implemented in COMSOL Multiphysics.

This section presents optimization problems with different objective functions. Initially the single objective funtion of minimizing viscous dissipation is used; this is followed by increasing the emphasis on heat transfer by using a weighted multi-objective function. Finally the single objective function of minimizing the outlet temperature is used. The thermal resistance of the optimized designs is used as a measure of thermal performance as it is independent of the inlet fluid temperature.

3.2.1 Design case 0: minimize $\phi_{\mathbf{T}}$

Design case 0 has the viscous dissipation in the objective function, and the optimization problem to minimize it is defined as

$$\begin{aligned} &\text{minimize} && \phi_{\mathrm{T}} \\ &\text{subject to} && 0 \leq \gamma_{\mathrm{i}} \leq 1 \end{aligned}$$

Figure 3.9 shows the density field of the design that minimizes viscous dissipation along with the streamline plot of the fluid. The white regions represent the fluid channel while streamlines are shown with blue lines.

Since the Reynolds number of the fluid is low, the viscous dissipation is minimized by increasing the channel width. The viscous dissipation of the topology optimized design is lower than the viscous dissipation of the reference design, while the thermal resistance of the design is higher. Table 3.5 compares the results of the optimization problem with the output of the reference design. The viscous dissipation in the optimized design is 1.96e-9 W, and all designs in this chapter are scaled with this number for comparison.

The temperature profile and heat flux in the y direction in the domain are shown in Figures 3.10 and 3.11. The heat flux is large near the cold plates due to convective heat transfer. This is also seen from the temperature profile as a large temperature gradient is present near the cold plates. The heat flux is also large near the outlet as the fluid converges to the outlet. The large flux is because the difference between the fluid and cold plate temperature is still significant near the exit, and the heat transfer coefficient of a narrower channel is higher.

Additionally, the thermal resistance of the optimized design is higher than that of the reference design, and the average outlet temperature of the fluid is 317.2 K in this design. The larger thermal resistance of the design is because the temperature at the outlet was excluded from the objective function of the optimization problem.

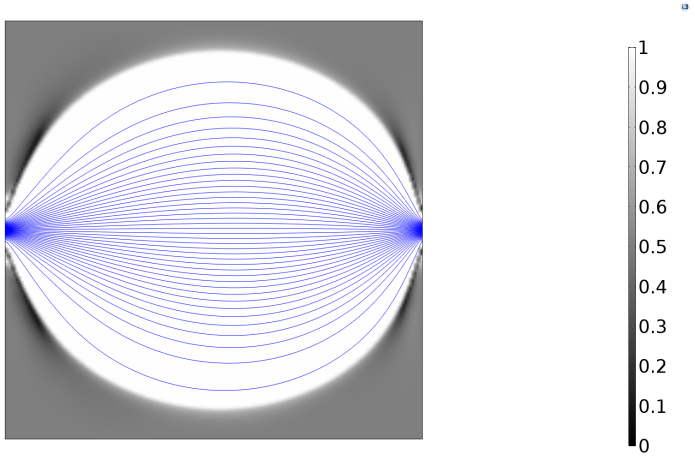

Figure 3.9: Case 0: density field (γ) and streamlines of the design that minimizes ϕ_{T}.

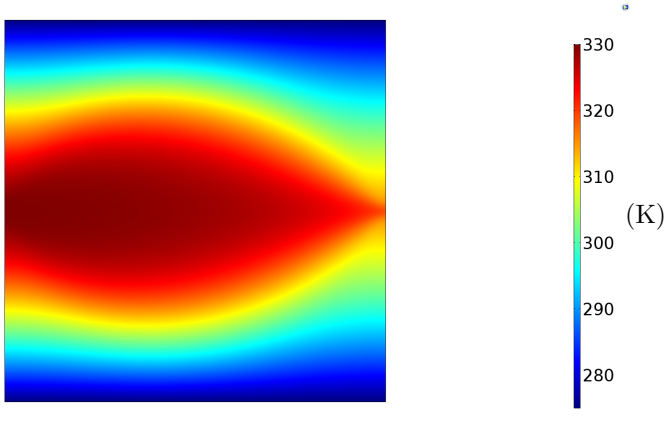

Figure 3.10: Temperature profile in the domain of the design that minimizes viscous dissipation.

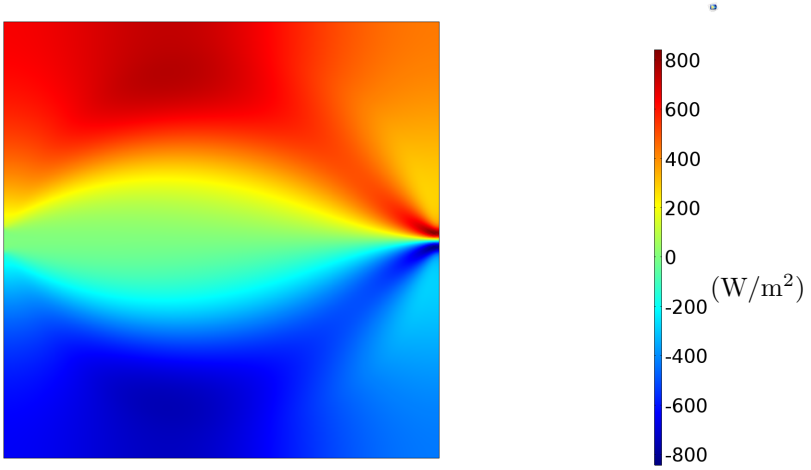

Figure 3.11: Heat flux in the vertical direction of the design that minimizes viscous dissipation.

Table 3.5: Comparison of design case 0 and the reference design.

Design	$\phi_{\text{d,scaled}}$	T_{o} (K)	R_{th}
Design case 0	1	317.2	0.271
Reference design	9.49	279.87	0.0313

The thermal performace of the topology optimized design is improved by using a multi-objective function, and increasing the weight on the thermal objective. The multi-objective optimization problem is defined as

$$\text{minimize} \qquad w_1 \frac{T_{\text{int}}}{c_1} + w_2 \frac{\phi_{\text{T}}}{c_2}$$

$$\text{subject to} \qquad 0 \leq \gamma_{\text{i}} \leq 1$$

Where T_{int} is the integral of the outlet temperature. An initial scaling is used to normalize T_{int} (c_1=2.5248) and ϕ_{T} (c_2=2.06e-9) with an initial design that has $\gamma = 0.5$ throughout the domain.

3.2.2 Design case 1: minimize f with $w_1 = 1$ and $w_2 = 1$

Design case 1 uses an objective function with equal weights on the two functions: $f = \frac{T_{\text{int}}}{c_1} + \frac{\phi_{\text{T}}}{c_2}$. Figure 3.12 shows the density field and streamlines of the optimized design. The design is similar to design case 0, and it has a wide central channel. The contact area between the fluid and cold plates has increased from design case 0 to increase heat transfer. The average outlet temperature of the fluid has decreased to 316.76 K, which is still higher than the average fluid temperature of the reference design. Therefore the weight w_1 is increased further.

3.2.3 Design case 2 minimize f with $w_1 = 100$ and $w_2 = 1$ and design case 3 minimize f with $w_1 = 5000$ and $w_2 = 1$

Design case 2 has an objective function with the temperature objective scaled a hundred times more than the viscous dissipation: $f = 100 \frac{T_{\text{int}}}{c_1} + \frac{\phi_{\text{T}}}{c_2}$. Figure 3.13 shows the density field and streamlines of the optimized design. The path taken by the fluid is the same as the reference design, but the channel thickness of the design is different from the channel thickness of the

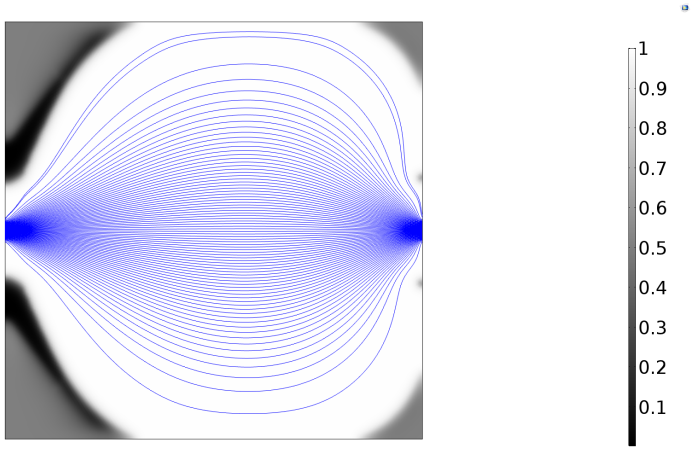

Figure 3.12: Case 1: density field (γ) and streamlines of the design optimized with $f = \frac{T_{\text{int}}}{c_1} + \frac{\phi_{\text{T}}}{c_2}$.

reference design. The heat transfer coefficient at the cold plates is different due to the difference in channel geometry, and the average fluid outlet temperature is 282.98K.

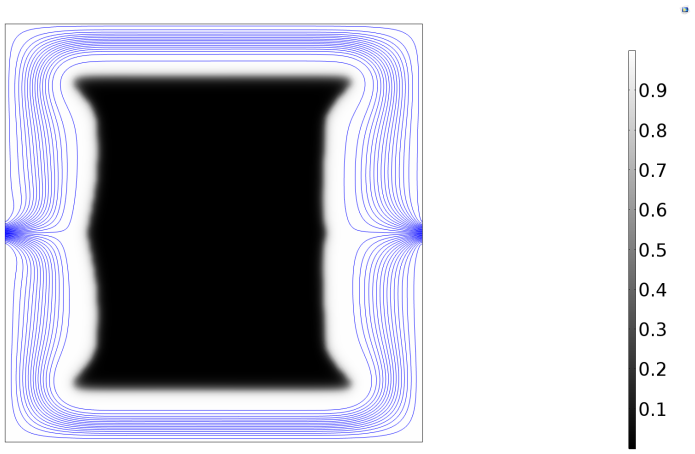

Figure 3.13: Case 2: density field (γ) and streamlines of the design optimized with $f = 100\ \frac{T_{\text{int}}}{c_1} + \frac{\phi_{\text{T}}}{c_2}$.

The weight on the temperature objective is further increased to five thousand for design case 3 to further improve thermal performance: $f = 5000\ \frac{T_{\text{int}}}{c_1} + \frac{\phi_{\text{T}}}{c_2}$. Figure 3.14 shows the density field and streamlines of the optimized design. The fluid channels are narrower in the present design when compared to design case 2 and the reference design. The average outlet temperature is lowered to 277.33 K in design case 3. This is due to an increase in heat transfer coefficient at the cold plates. Figure 3.15 compares the heat transfer coefficient between the reference design and design cases 2 and 3 at the top plate. Design case 3 has a higher heat transfer coefficient than design case 2 or the reference design. Therefore the average outlet temperature of design case 3 is the lowest.

The above approach demonstrates that topology optimization can be used to tune the geometry of fluid channels to arrive at the optimal trade off between viscous dissipation and thermal resistance. However, this approach requires a few attempts to arrive at suitable weights to find the final design. This approach is costly when attempting to solve a 3d optimization problem as the model evaluations become expensive. Moreover, the constraint form of the optimization problem can be used to arrive at a design that meets the performance requirements directly by explicitly adding the viscous dissipation as a constraint.

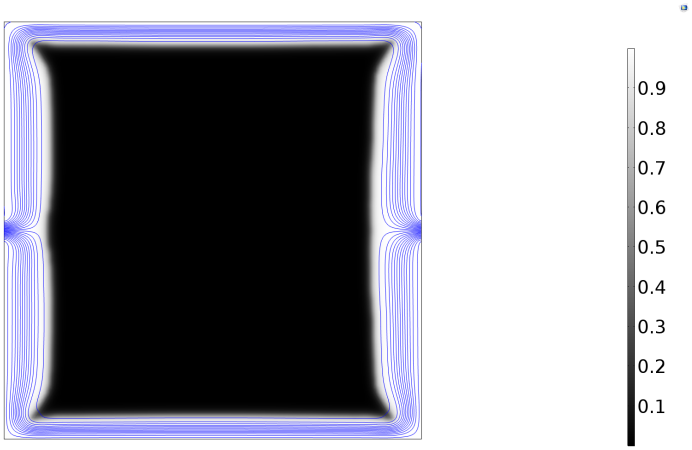

Figure 3.14: Case 3: density field (γ) and streamlines of the design optimized with $f = 5000\ \frac{T_{\text{int}}}{c_1} + \frac{\phi_{\text{T}}}{c_2}$.

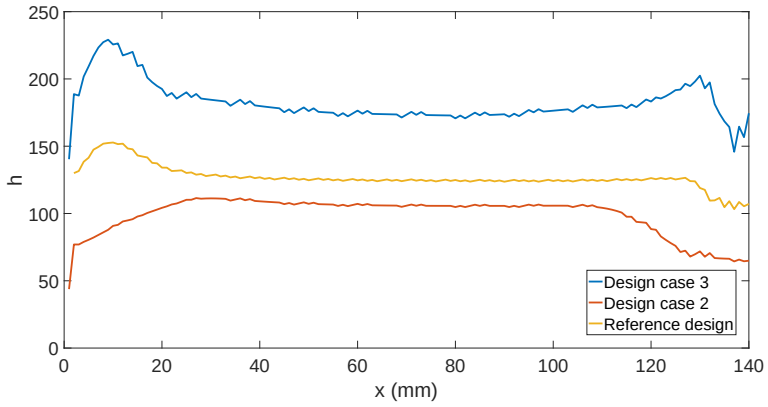

Figure 3.15: Comparison of the heat transfer coefficients between the reference design and design cases 2 and 3 at the top plate. The heat transfer coefficient scales directly with channel width, and the channel width of a design is reduced as the weight on the thermal objective is increased.

3.2.4 Design case 4: minimize T_{int}

Design case 4 has a single objective function that minimizes the average outlet temperature: $f = T_{\text{int}}$. Figure 3.16 shows the density field and streamlines of the optimized design. The average outlet temperature of the fluid is 275.28 K, and the thermal resistance of this design is lower than all the previous designs.

In addition to narrow channels at the cold plate, the design minimizes the outlet temperature by increasing the area of heat transfer. The fluid flows to the top plate initially. It is then directed to the bottom plate with additional fluid channels. The area of heat transfer is increased as there is convective heat transfer in the horizontal direction in the additional vertical channels.

Figure 3.17 shows the convective product in the y-direction. It shows that heat is lost by convection as the fluid flows in the additional vertical channel. Additionally, Figure 3.18 shows the horizontal heat flux in the domain; it shows the horizontal convective flux due to the vertical channels. The vertical channels to the bottom plate also have holes that splits the fluid into two paths. This reduces the effective channel width and increases the heat transfer coefficient in the horizontal direction. The left side of the vertical channels gain heat from the inlet, while the right side loses heat towards the outlet. The heat gained in the vertical channels is then lost at the bottom plate.

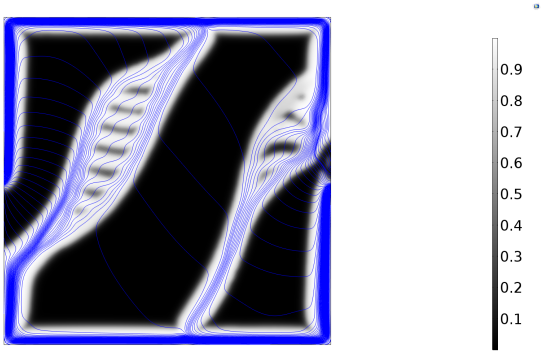

Figure 3.16: Case 4: density field (γ) and streamlines of the design optimized with $f = T_{\text{int}}$.

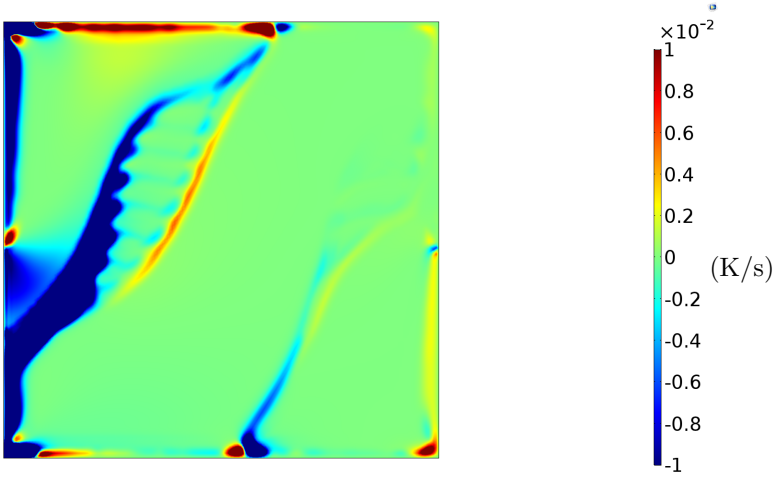

Figure 3.17: Convective product in the vertical direction show convection heat transfer in the vertical fluid channels.

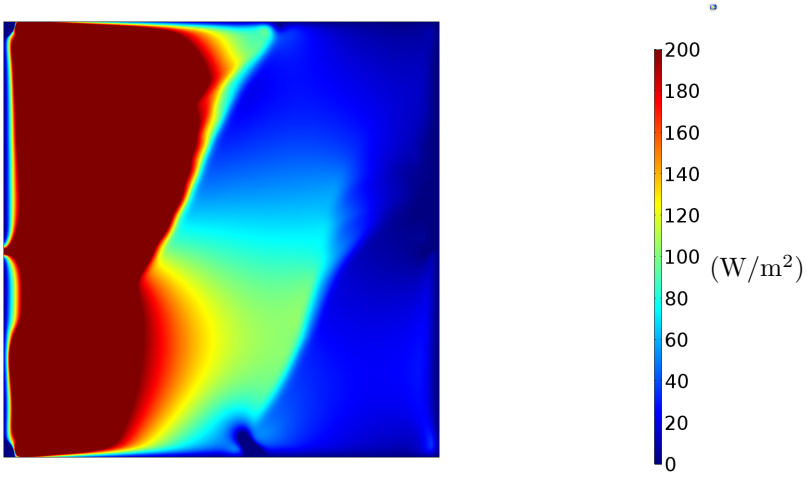

Figure 3.18: Heat flux in the horizontal direction that show the heat lost and gained by the fluid in the vertical channels.

The fluid stream also mixes flowing while flowing from right to left because of the holes in the vertical channels. This results in vertical heat flux due to convection. The regions with convective flux are seen from the convective product in Figure 3.19, and Figure 3.20 shows the convective heat flux due to the horizontal flow. The vertical flux equalizes the temperature profile in the x-direction as the fluid reaches the left side of the vertical channel. This creates the entrance effect

leading to higher heat transfer coefficients in the vertical channels.

Table 3.6 compares the thermal resistance of the optimized designs for different objective functions. The designs with an increased weight on T_{int} have a lower thermal resistance. The decrease in thermal resistance is due a reduction in channel width as well as an increase in the area of heat transfer. However the design trade-off is that both the above factors lead to an increase in viscous dissipation.

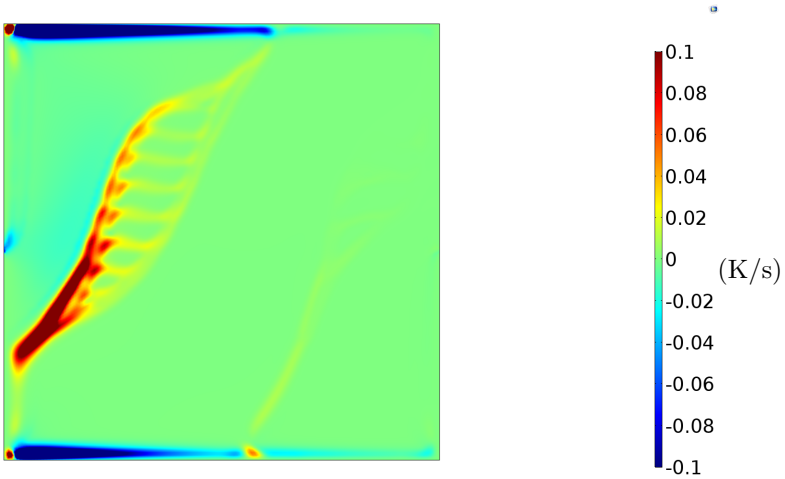

Figure 3.19: Convective product in the horizontal direction shows convection heat transfer due to horizontal flow because of the holes in the vertical channel.

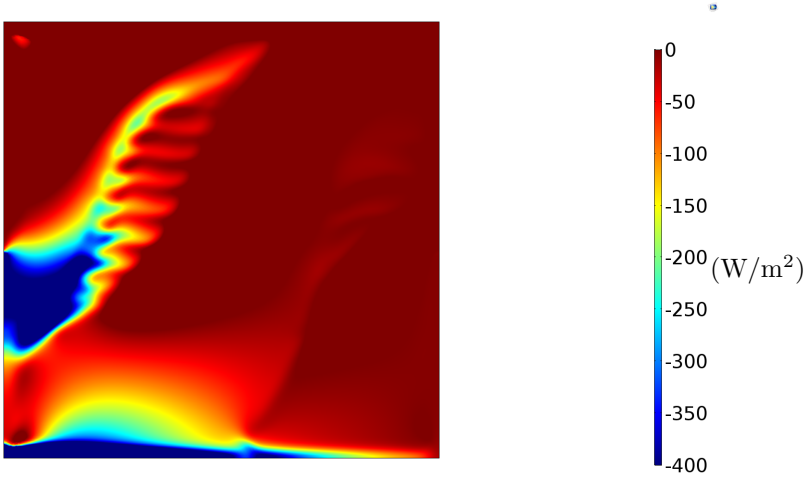

Figure 3.20: Heat flux in the vertical direction shows heat transfer to equalize temperature due to horizontal flow because of the holes in the vertical channel.

3.2.5 Penalization of flow through porous regions

Design cases 1 to 3 have a term in the objective function that penalizes flow through porous regions (ϕ_α). The topology optimized designs of the respective designs show an increase in ϕ_α as w_1 is increased (see Table 3.7), which means more fluid flows through the porous solid. However, design case 4 does not penalize porous flow in the objective (flow through porous regions is maximum in this design). Yet the optimized design has a fluid flow path from inlet to outlet. This is due to the nature of the combined optimization problem of fluid flow and convective heat transfer.

Solid elements dampen velocities with a large penalization parameter (α_{max}), and they are used to control the direction and magnitude of the velocity at different locations in the design domain. Regions near the cold plate have narrow regions with no velocity penalization (or α_{min}) surrounded

Table 3.6: Viscous dissipation, outlet temperature and thermal resistance of the topology optimized designs with different objective functions are compared.

Objective function	$\phi_{\mathrm{d,scaled}}$	T_{o} (K)	R_{th}
ϕ_{T}	1	317.2	0.271
$\frac{T_{\mathrm{int}}}{c_1} + \frac{\phi_{\mathrm{T}}}{c_2}$	1.003	316.76	0.261
$100\ \frac{T_{\mathrm{int}}}{c_1} + \frac{\phi_{\mathrm{T}}}{c_2}$	3.11	282.98	0.038
$5000\ \frac{T_{\mathrm{int}}}{c_1} + \frac{\phi_{\mathrm{T}}}{c_2}$	15.17	277.33	0.022
T_{int}	142.14	275.28	0.0136
Reference design	9.49	279.87	0.0313

by solid regions with $\alpha_{\max}$ to simulate a narrow channel. Narrow fluid channels increase convective heat transfer. Therefore the topology optimized designs prefer a clear separation of solid and fluid regions to maximize convective heat transfer and minimze the outlet temperature.

The clear separation of solid and fluid regions is also obtained due to the nature of design domain. The 2d domain defined in this chapter has a cold plate stretching from the inlet to the outlet. The solution of design case 4 has a connection from the bottom cold plate to the outlet so that fluid does not short circuit to the outlet before the end of the cold plate. This ensures optimal use of the fluid for heat transfer.

Table 3.7: Comparison of the porous flow product (ϕ_α) of the 2d topology optimized designs.

Design case	ϕ_α
Case 1	1.38e-11
Case 2	1.27e-9
Case 3	1.63e-9
Case 4	1.11e-6

3.3 Post-processing of model to validate the optimization routine

The topology optimized designs are post-processed by exporting the density field of the designs. Fluid regions within the domain are filtered using the criteria $\gamma \geq 0.8$. The fluid channel geometry is traced with a spline function in SOLIDWORKS using the spatial distribution of the filtered densities. The post-processed designs are simulated using the same boundary conditions and mesh used in the optimization model. The results of both models are finally compared.

The fluid channels of the post-processed designs are the blue regions in Figure 3.21. Table 3.8 compares the fluid outlet temperatures and viscous dissipation in the designs. The outlet temperatures and viscous dissipation of a model are identified from the subscript. The difference in solutions exist as the no-slip boundary condition is not exact in the porous flow model. This results in different velocity profile in the channel that leads to different heat transfer coefficients and pressure drops in a channel.

The porous flow models simulate narrower fluid channels. Therefore, the outlet temperatures found using the porous flow model are lower while the viscous dissipation is higher. Design case 1 is an exception as the area of contact between the fluid channels and cold plates increase in this design, which results in a lower outlet temperature in the post-processed design. The post-processing criteria is not made more strict in order to capture all the details of the designs.

The results are consistent with objective functions used in the optimization model. The designs show an improvement in thermal performance as the weight on the thermal objective is increased.

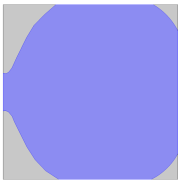

(a) Post-processed design case 1

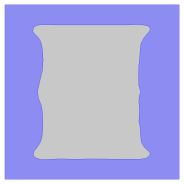

(b) Post-processed design case 2

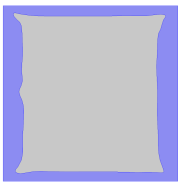

(c) Post-processed design case 3

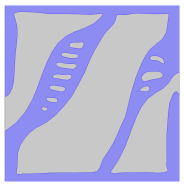

(d) Post-processed design case 4

Figure 3.21: Geometry of the post-processed topology optimized designs using the criteria $\gamma \geq 0.8$.

The results also validate the use of the porous flow model to optimize the channel geometries within the design domain.

Table 3.8: Comparison of viscous dissipation and outlet temperatures of the optimized designs after post-processing.

Design case	$\phi_{\mathrm{d,porous}}$ (W)	$\phi_{\mathrm{d,fluid}}$ (W)	$T_{\mathrm{o,porous}}$ (K)	$T_{\mathrm{o,fluid}}$ (K)
Case1	1.97e-9	1.92e-9	316.76	316.25
Case2	6.1e-9	3.94e-9	282.98	287.44
Case3	2.76e-8	2.5e-8	277.33	277.89
Case4	2.8e-7	1.36e-7	275.28	276.26

Chapter 4

Topology optimization of a convective cooling system with separation of fluid and solid conductivities in design domain

A metal heat exchanger is generally designed with fins to increase the area of contact between the fluid and the metal. Metals with large conducivity spread heat effectively, enabling heat exchanger designs with a low thermal resistance. The current heat exchanger at ASML uses Peltier elements to exchange heat with the fluid. Metal fins can be connected close to these Peltier elements to reduce the thermal resistance of the heat exchanger.

The 2d design domain defined in Chapter 3 is used to find heat exchanger designs in this chapter. Additionally, solid regions are assigned the conductivity of Aluminum, while the fluid regions are assigned the conductivity of water. The goal of the topology optimization problem is the same as the goal of Chapter 3: find a design with a lower thermal resistance than the reference design. The geometry of the reference design is the same as the geometry as the reference design in Chapter 3.

The multi-objective formulation is initially used to find topology optimized designs. This is followed by the single objective case of minimizing the outlet temperature with a constraint on the viscous dissipation in the design. In the constraint form of the optimization problem the optimizer exploits the density based conductivity interpolation model described in Chapter 2. The observation is illustrated with a numerical example. Finally solution startegies to resolve the issue are discussed.

The dimensions of the design domain, optimization parameters and the properties of water are the same as in Chapter 3, while the conductivity of aluminum is defined as 205 W/(m-K).

4.1 Reference design to the optimization problem

The reference design to the optimization problem is the same as in Chapter 3. The solid regions of the reference design in this chapter have the conductivity of aluminum. This results in a large amount of heat conducted towards the outlet. Figure 4.1 shows the temperature profile in the domain. The temperature gradient in horizontal direction is lower than the gradient present in the reference design of Chapter 3 i.e. the heat lost to the cold plates is lesser. Therefore the outlet temperature (292.9 K) of this design is higher than the outlet temperature of the previous reference design (279.85 K). The viscous dissipation is unaffected by the addition of the conductivity of the solid.

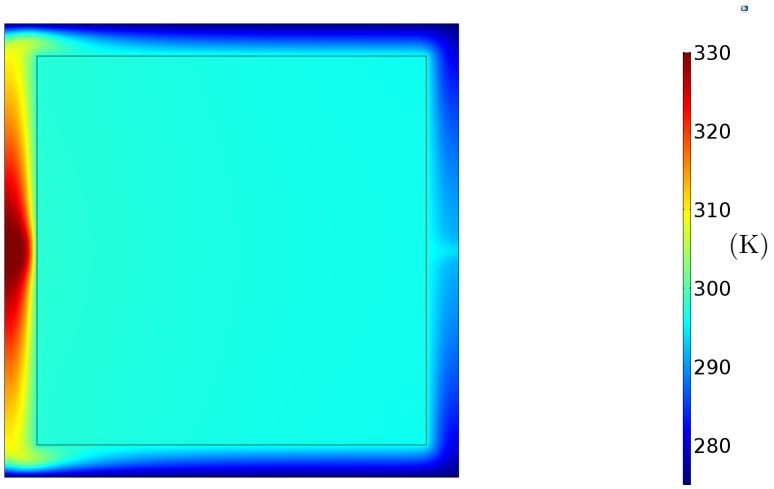

Figure 4.1: Temperature profile in the 2d reference design. The large conductivity of aluminum causes only a small temperature gradient in the horizontal direction resulting in less heat lost to the cold plates.

4.2 Topology optimization of the design

The optimization model allocates a conductivity coefficient to each element in the design domain. Conductivity is allocated in a similar manner to the Brinkman penalization parameter (α). It is defined using a RAMP interpolation function in the following manner:

$$k = k_{\text{Al}} + (k_{\text{water}} - k_{\text{Al}})\gamma(\frac{1+q}{\gamma+q}), \tag{4.1}$$

where k_{water} is the conductivity of water and k_{Al} the conductivity of aluminum. The same interpolation parameter q is chosen for both α and k. The conductivity of a material is used in the convection diffusion equation defined in Equation 2.18 to determine the temperature field in the domain. The objective function of the optimization problem is the multi-objective function $f = w_1\frac{T_{\text{int}}}{c_1} + w_2\frac{\phi_{\text{T}}}{c_2}$. The weights of the objective function are tuned to find a design with a lower thermal resistance than the reference design.

4.2.1 Design case 1: minimize f with $w_1 = 1$ and $w_2 = 1$

Design case 1 has equal weights on both functions of the objective: $f = \frac{T_{\text{int}}}{c_1} + \frac{\phi_{\text{T}}}{c_2}$. Figure 4.2 shows the density field and streamlines of the optimized design. The design is similar to design case 0 of Chapter 3. In addition to the corresponding design in Chapter 3, this design also has high conductivity metal fins close to the inlet and outet (see the conductivity distribution in Figure 4.3). These fins provide a low resistance heat flux path to the cold plates. Figure 4.4 shows the vertical heat flux in the domain, and the flux carried by the fins to the cold plate is seen. They improve the thermal performance of the design, and the average fluid outlet temperature of the fluid is 299.45 K.

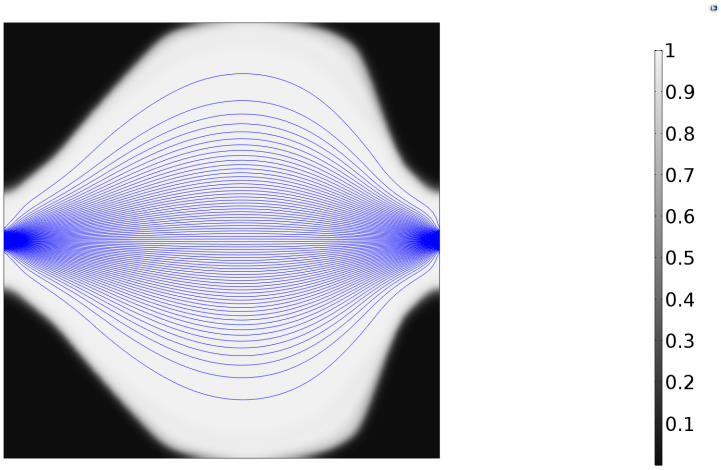

Figure 4.2: Case 1: density field and streamlines of the design optimized with $f = \frac{T_{\text{int}}}{c_1} + \frac{\phi_{\text{T}}}{c_2}$.

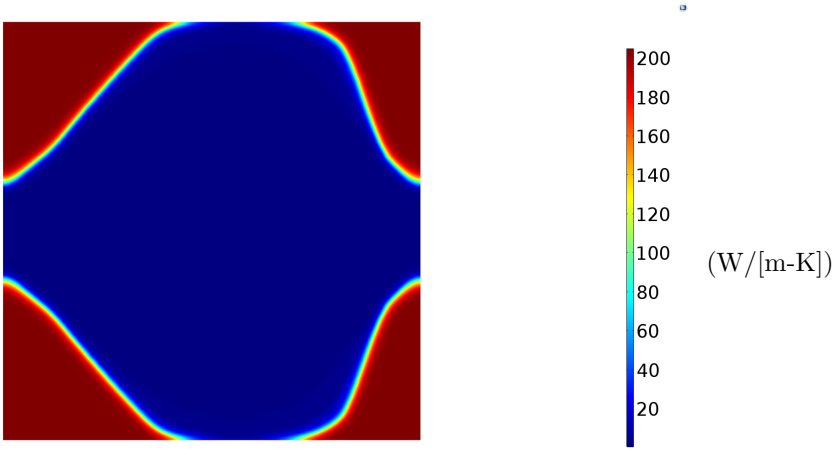

Figure 4.3: Case 1: conductvity distribution of the design optimized with $f = \frac{T_{\text{int}}}{c_1} + \frac{\phi_{\text{T}}}{c_2}$.

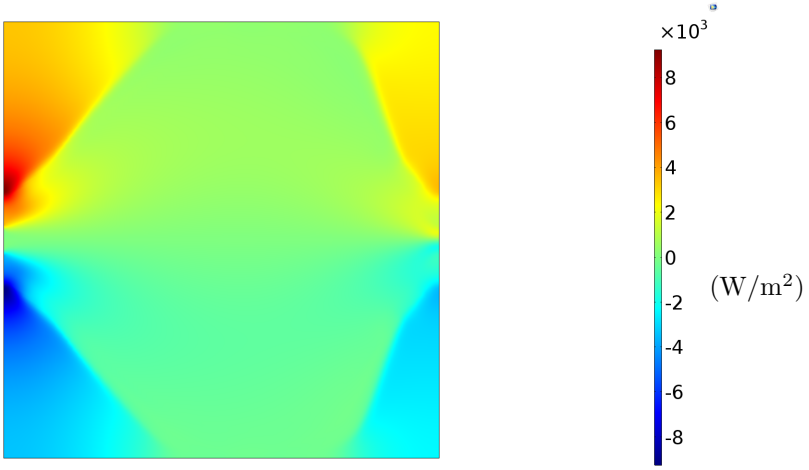

Figure 4.4: Heat flux in the vertical direction shows a large amount of heat diffusing through the metal fins.

4.2.2 Design case 2: minimize f with $w_1 = 100$ and w_2=1

Design case 2 has the temperature objective scaled 100 times more than ϕ_T: $f = 100\ \frac{T_{int}}{c_1} + \frac{\phi_T}{c_2}$. Figure 4.5 shows the density field and streamlines of the optimized design. The design has horizontal fluid channels at the cold plates for convective heat transfer, which are also present in the reference design. The design also has a central cavity with the conductivity of the fluid, however no fluid flows through this region, which is seen from the streamlines in Figure 4.5. The low conductivity region reduces the heat flux via conduction in the horizontal direction resulting in more heat transfer at the cold plates.

In addition to the convective flux in the horizontal channels, the design has metal fins near the inlet and outlet connected to the cold plates. They provide a low resistance path for the flux to the cold plates. The vertical heat flux in the domain is shown in Figure 4.7. The average outlet fluid temperature is 281.67 K, which is below the reference design's average outlet temperature.

The above designs use aluminum to create fins that increase the area of heat transfer within the design domain, however there is additional space in the domain that can be used to further improve the thermal performance. Hence the thermal objective is further scaled to study the impact on the design.

4.2.3 Design case 3: minimize f with $w_1 = 5000$ and $w_2 = 1$

Design case 3 has the temperature objective scaled 5000 times more than ϕ_T: $f = 5000\ \frac{T_{int}}{c_1} + \frac{\phi_T}{c_2}$. Figure 4.8 shows the density field and streamlines of the optimized design. The design has a fluid channel that initially directs the fluid to the bottom cold plate. It then flows to the top cold plate and finally to the outlet.

Metal fins are placed against the top and bottom cold plates as seen in Figure 4.9. They remove heat from the fluid as it flows in both the horizontal and vertical channels. The fins conduct heat in the vertical direction to the cold plates. Figure 4.10 shows the vertical heat flux carried by the fins. The fins also increase the area of heat transfer of the fluid channels in the domain.

In addition to the fins the design has metal fillings in the fluid channel that create 2 narrow channels in the vertical path, which increases the heat transfer coefficient of the channels. The fillings also cause horizontal fluid flow that equalizes the temperature profile of the fluid similar to design case 4 of Chapter 3. This results in a higher heat transfer coefficient locally, similar to the thermal entrance region. These design features create a low thermal resistance design, and the average outlet fluid temperature is 275.61 K. Table 4.1 compares the thermal resistance of and viscous dissipation in the topology optimized designs using different objective functions. The optimization model performs as expected as the thermal performance of the designs increase when the weight on the thermal objective is increased along with an increase in viscous dissipation. Design cases 2 and 3 have a lower thermal resistance than the reference design. These designs use metal fins to increase the area of heat transfer and provide a low resistance flux path to the cold plates.

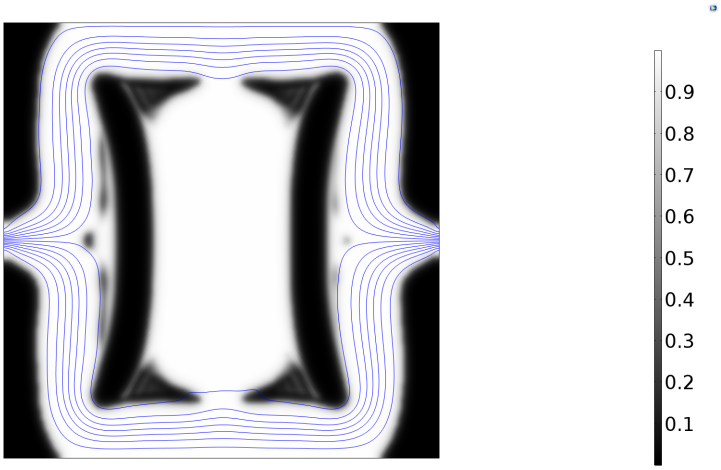

Figure 4.5: Case 2: density field and streamlines of the design optimized with $f = 100\ \frac{T_{\text{int}}}{c_1} + \frac{\phi_{\text{T}}}{c_2}$.

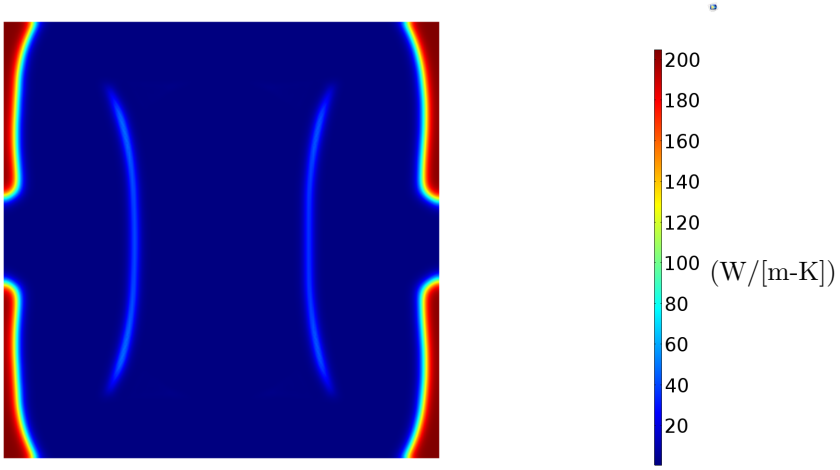

Figure 4.6: Case 2: conductvity distribution of the design optimized with $f = 100\ \frac{T_{\text{int}}}{c_1} + \frac{\phi_{\text{T}}}{c_2}$.

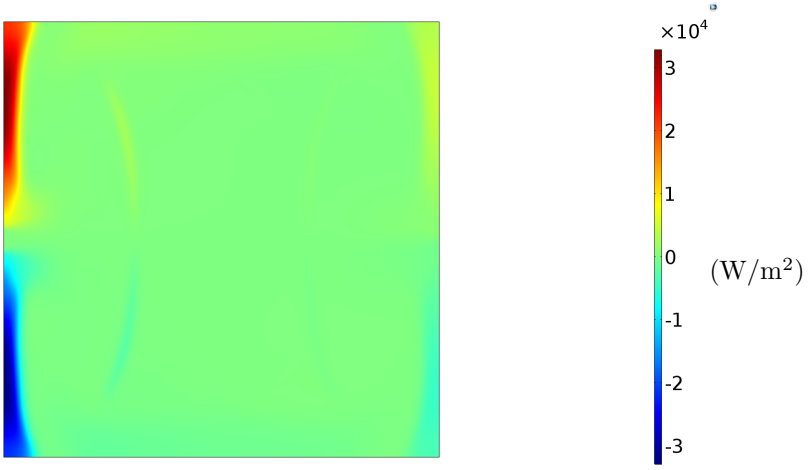

Figure 4.7: Heat flux in the vertical direction.

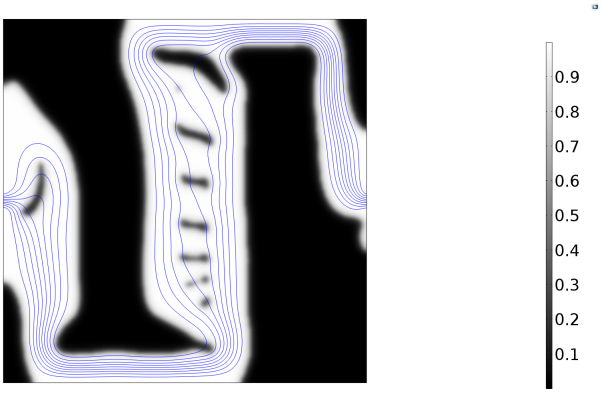

Figure 4.8: Case 3: density field and streamlines of the design optimized with $f = 5000\ \frac{T_{\text{int}}}{c_1} + \frac{\phi_{\text{T}}}{c_2}$.

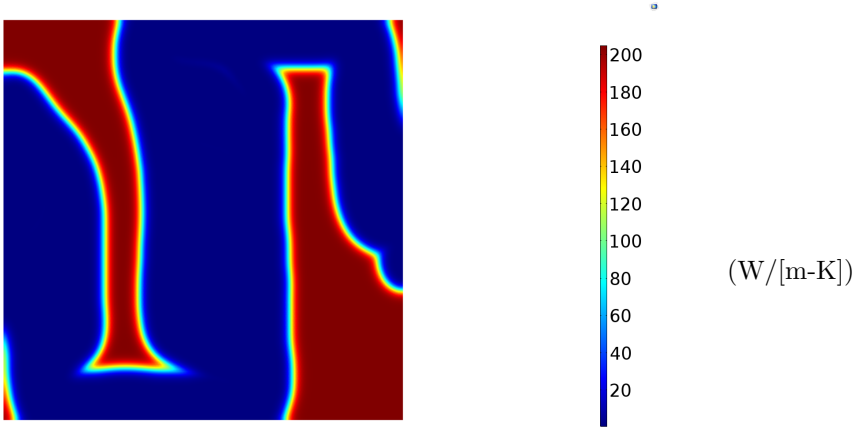

Figure 4.9: Case 3: conductvity distribution of the design optimized with $f = 5000\ \frac{T_{\text{int}}}{c_1} + \frac{\phi_{\text{T}}}{c_2}$.

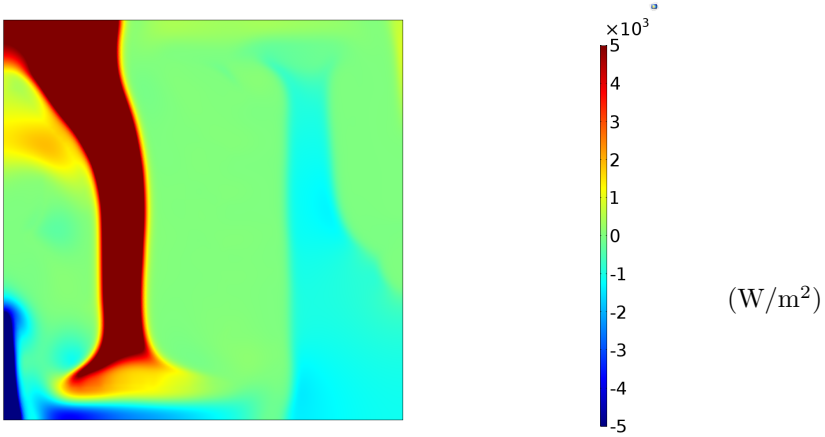

Figure 4.10: Heat flux in the vertical direction shows a large amount of heat diffusing through the metal fins. The metal fins also increase the area of heat exchange of the fluid channels in this design to improve the thermal performance.

Table 4.1: Thermal resistance of and viscous dissipation in the topology optimized designs with the conductivity interpolation model using different objective functions.

Objective function	$\phi_{\mathrm{d,scaled}}$	T_{o} (K)	$\mathrm{R_{th}}$
$\frac{T_{\mathrm{int}}}{c_1} + \frac{\phi_{\mathrm{T}}}{c_2}$	1.015	299.45	0.089
$100\ \frac{T_{\mathrm{int}}}{c_1} + \frac{\phi_{\mathrm{T}}}{c_2}$	1.84	281.67	0.034
$5000\ \frac{T_{\mathrm{int}}}{c_1} + \frac{\phi_{\mathrm{T}}}{c_2}$	8.06	275.61	0.0016
Reference design	9.49	292.9	0.064

4.3 Design case 4: minimize $T_{\mathbf{int}}$ subject to a constraint on $\phi_{\mathbf{d}}$

The viscous dissipation in the reference design is used as a constraint in the next optimization routine to study the impact of including the conductivity interpolation with the single objective function of minimizing the outlet temperature.

The constraint form of the optimization problem is defined to avoid a trial and error approach of using different weights using the multi-objective approach to find a design that performs better than the reference design. The viscous dissipation in the reference design is used as the upper bound on the constraint on viscuous dissipation in the design. The optimization problem is defined as

$$\begin{aligned} &\text{minimize} && T_{\mathrm{int}} \\ &\text{subject to} && \phi_{\mathrm{d}}/(1.8e-8) \leq 1 \\ & && 0 \leq \gamma_{\mathrm{i}} \leq 1 \end{aligned}$$

4.3.1 Results

Figure 4.11 shows the density distribution and streamline plot of the topology optimized design. The design has 2 vertical strips of aluminum connecting the top and bottom cold plates, with no exclusive fluid channel. Therefore, the fluid flows through the porous strip towards the outlet as seen from the streamline plot in Figure 4.11.

Figure 4.12 shows the conductivity distribution within the domain. The solid strips have the conductivity of aluminum in this design. The velocity of the fluid does not become zero in the porous solid leading to large convective transport in the horizontal direction. This is seen from the convection diffusion equation of a fluid:

$$\rho_{\mathrm{f}} C_p \boldsymbol{v}.\nabla \mathrm{T} - k_{\mathrm{f}} \nabla^2 T = 0, \tag{4.2}$$

however the current model has the conductivity of the solid in the place of the fluid changing the above equation to

$$\rho_{\mathrm{f}} C_p \boldsymbol{v}.\nabla \mathrm{T} - k_{\mathrm{s}} \nabla^2 T = 0. \tag{4.3}$$

The average outlet temperature is low as a result of the increased convective transport.

The blue strip in Figure 4.13 shows the large reduction in energy of the fluid as it hits the vertical strip of solid. The energy lost by the fluid is conducted in the vertical direction to the cold plates as seen from the vertical heat flux plot of Figure 4.14. The optimization model takes advantage of the porous flow model, and it allocates the design variable so that convective transport is achieved with the conductivity of the solid. However this design is infeasible and since such a material does not exist.

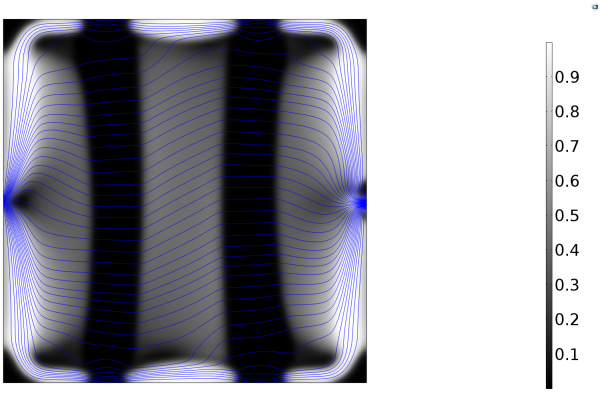

Figure 4.11: Density field (γ) and streamlines of the design optimized to minimize outlet temperature. The streamlines show that a large amount of porous flow is present in this design.

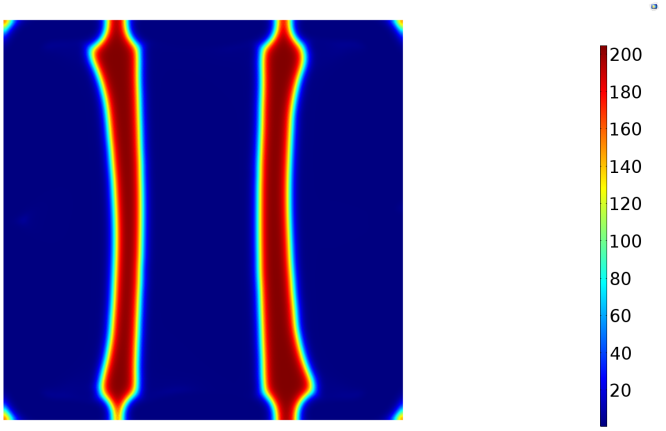

(W/[m-K])

Figure 4.12: Conductvity distribution of the design optimized to minimize outlet temperature. The design makes use of porous flow at large conductivities to mazimize heat transfer.

(K/s)

Figure 4.13: Convective product in the x-direction (uT_{x}) shows the large reduction in the energy of the fluid as the fluid flows through the highly conductive region.

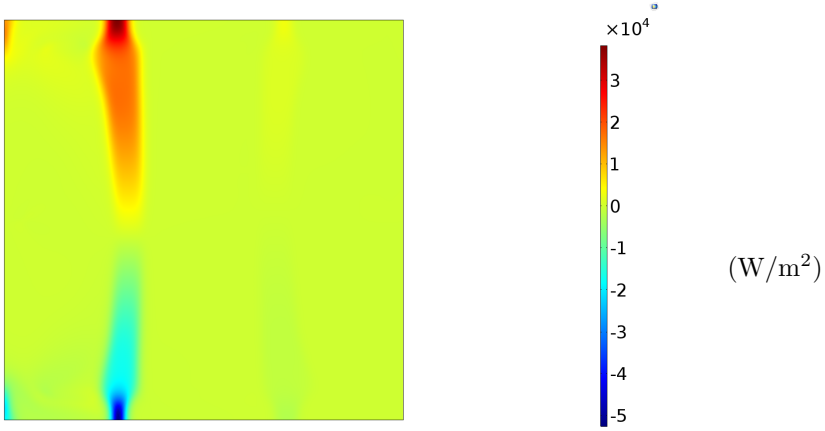

Figure 4.14: Heat flux in the y-direction shows the heat removed by the highly conductive porous solid.

4.4 Discussion

The constraint form of the optimization model does not utilize the porous flow product (ϕ_α) in either the objective function or the constraint. The optimized design has a large amount of porous flow in the above design and ϕ_α is 1.037e-6. The optimization problem can be formulated with the porous flow product in the objective to find a feasible design. The optimization problem can be defined as

$$\begin{aligned} &\text{minimize} && \mathrm{w}_1 \, \frac{T_{\mathrm{int}}}{c_1} + \mathrm{w}_2 \, \frac{\phi_\alpha}{c_2} \\ &\text{subject to} && \phi_{\mathrm{d}}/(1.8e-8) \leq 1 \\ & && 0 \leq \gamma_{\mathrm{i}} \leq 1. \end{aligned}$$

However the above approach can lead to a local optima as the weight on the porous flow product is subjective. The porous flow product of design case 4 in Chapter 2 is 1.11e-6, which is higher than the porous flow product of the current design. However design case 4 of Chapter 3 is still feasible with well defined fluid channels from inlet to outlet.

The numerical issue found in the constraint form of the problem can be avoided using a heuristic approach, where the porous flow product is used in the objective function. The weight w_2 on ϕ_α can be reduced after a given number of iterations. The weight is reduced if the design is feasible to avoid a local optima. However this approach is cumbersome as it requires intervention between optimization steps.

The current model has the conductivity of an element defined as a function of the design variable in the interpolation function, while porous flow is also allowed. The conductivity of an element is additionally a function of the average velocity in an element as well, where solid regions have zero velocity. Chapter 5 defines a conductivity distribution model based on the velocity of a fluid element.

Chapter 5

Alternate conductivity model for the design of convective cooling systems

Chapter 4 illustrates the erosion of the convection diffusion optimization model when ϕ_α is excluded from the objective function. A case for excluding it from the objective function is also made. This chapter presents a conductivity model as a function of the velocity field. This is followed by a 2d numerical example to validate the approach.

The optimization model defined in Chapter 4 has conductivity defined as a function of the design variable. This approach is based on the assumption that elements with a large penalization (α) on velocity have a low velocity. However the velocity field depends on the allocation of α in the neighbourhood of an element as well.

The optimization algorithm maximizes convective heat transfer via porous flow through large conductivities with the density based conductivity interpolation model. This model results in infeasible designs though the viscous dissipation (ϕ_d) in the designs are low. Penalizing porous flow by adding ϕ_α in the objective function can prevent infeasible designs depending on the scaling of weights in the multi-objective function: $f = w_1 \frac{T_\mathrm{int}}{1} + w_2 \frac{\phi_\alpha}{c_2}$.

The new model has conductivity defined as a function of the velocity field to ensure that porous flow is undesired in the model to minimize thermal resistance. This approach is chosen to ensure that porous flow does not have to be penalized explicitly. A region with porous flow in the new model will have low conductivity, hence convective and conductive heat transfer is small in these regions. While a clear separation of solid and fluid regions will enable the optimal use of the conductive heat transfer in the solid as well as convective heat transfer in the fluid.

5.1 Conductivity model

The convection-diffusion problem studied has the conductivity of the solid larger than the conductivity of the fluid. The mode of heat transfer in the solid is conduction. While the mode of heat transfer in the fluid is conduction and convection, with convection heat transfer dominating over conduction. An optimization model is defined with the conductivity field defined as a continuous function of the velocity field in this section. This approach allows 0-1 topology optimized solutions without an explicitly large penalization on porous flow, while using a continuous optimization algorithm.

The definition of conductivity as a function of velocity poses the risk of fluid regions having different conductivities at different regions in the domain based on the geometry of the channel. Diffusive heat transfer is ill-defined in this case. Therefore, the chosen function requires a steep transition from the conductivity of the solid to the conductivity of the fluid, and remain constant

at large velocities. The analytical approximation to the heavyside function is used to define the conductivity distribution in the domain. The heaviside function of the fluid velocity is defined as

$$H = f(\boldsymbol{a}), \tag{5.1}$$

where H is the Heaviside function and $\boldsymbol{a}$ is a linear scaling of the velocity field from 0 to 1. The maximum channel velocity, $v_{\max}$, is defined using the minimum channel width in a design.

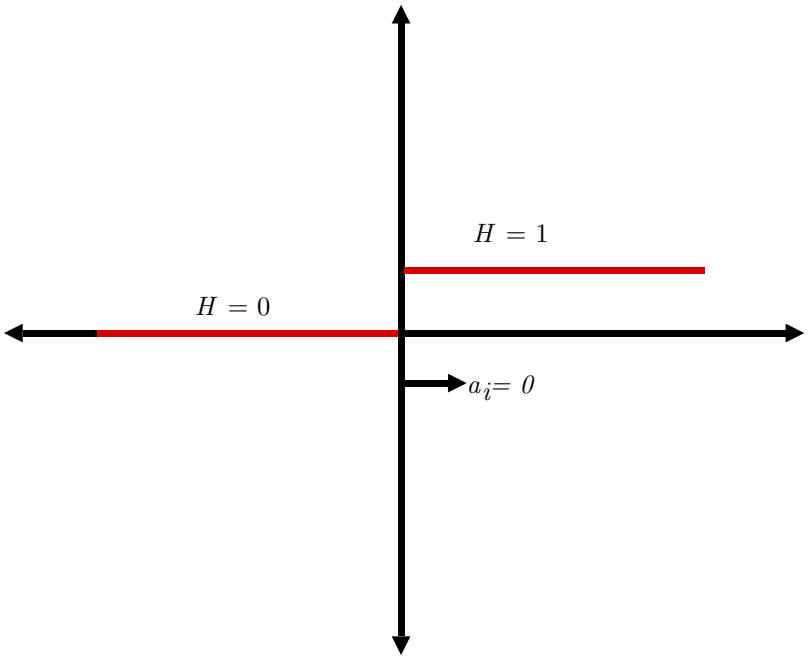

Figure 5.1: Discrete form of the Heaviside function centered at 0. Condutivity of an element is the conductivity of the solid when a_i is zero, and its the conductivity of the fluid if $a_i \geq 0$ in the discrete form of the new formulation.

Figure 5.1 shows the discrete form of the Heaviside function. It is approximated using an analytical function to make the it a continuous function of the velocity field. The analytical approximation of H at $\boldsymbol{a} = 0$ is

$$H(\boldsymbol{a}) = \frac{1}{1 + e^{-2t\boldsymbol{a}}}, \tag{5.2}$$

where t is a parameter that defines how fast H transitions from 0 to 1. The current optimization problem requires t be large for a steep transition of H so that the conductivity of the fluid has minimal perturbation.

The Heaviside function is centered at 0, it is 0.5 at zero velocity, and 1 at $\boldsymbol{v}_{\max}$ in the analytical approximation. The boundary conditions of the Heaviside function are

$$H(0) = 0.5 \quad \text{and} \tag{5.3}$$

$$H(1) = 1. \tag{5.4}$$

The conductivity distribution in the domain is defined as a linear function of H: $\boldsymbol{k}$ (H) i.e.

$$k_i(H) = c_3 H + c_4, \tag{5.5}$$

where k_i is the conductivity assigned to an element. The constants c_3 and c_4 are defined to satisfy the following boundary conditions:

$$k_i(0.5) = k_{\mathrm{s}} \quad \text{and} \tag{5.6}$$

$$k_i(1) = k_{\mathrm{f}}. \tag{5.7}$$

5.2 Numerical example

The design domain defined in Chapter 3 is used for the numerical example to demonstrate the conductivity interpolation model. The optimization problem is defined to minimize the outlet temperature of the fluid.

The parameters used in the optimization model are given in Table 5.1. The parameter $v_{\max}$ is chosen as the maximum fluid velocity in a 4 mm channel. The parameters c_3 and c_4 define k to transition from the conductivity of aluminum to water in Equation 5.5. The parameter t is chosen as 300 for a steep transisition in the Heaviside function to ensure diffusion in the fluid regions is modeled accurately. It can be alloted a larger magnitude, however this increases the risk of ending up at a local optima.

Table 5.1: Parameters used in the velocity interpolation optimization model.

Parameter	Magnitude
$\boldsymbol{v}_{\max}$	0.0017 m/s
c_3	-408.8
c_4	409.4
t	300

The optimization problem is defined as

$$\begin{aligned} &\text{minimize} && T_{\text{int}} \\ &\text{subject to} && 0 \leq \gamma_{\text{i}} \leq 1, \end{aligned}$$

The density field and streamlines of the design optimized using the velocity interpolation formulation is shown in Figure 5.2. The fluid channel has a serpentine like structure in order to increase the area of heat transfer in the domain. The density field however has regions with intermediate densities in the domain. These regions have not converged to 0 or 1 as they do not affect the flow direction. Moreover, conductivity is only a function of velocity so intermdiate densities do not affect the thermal resistance of the design either. The average outlet temperature of the fluid is 275.02 K and the viscous dissipation is 8.26e-8 W.

Figure 5.3 shows the conductivity field filtered using the criteria $k \leq$0.62 W/(m-K) to map the conductivity of the fluid, while the actual conductivity of the fluid is 0.6 W/(m-K). The regions that match this criteria map out the fluid path, which means that the conductivity allocated to the fluid has minimal perturbation. This also shows that heat transfer in the fluid regions is modeled accurately.

Figure 5.4 shows the conductivity distribution in the domain. The regions outside the fluid channel have a large conductivity, and they provide a low resistance path for the heat flux to the cold plates. Figure 5.5 shows the flux carried by the metal fins to the cold plates in the vertical direction.

The conductivity in regions where the fluid channels bend is below that of the solid because there is some leakage through the solid in these regions. However when the design was post-processed using the criteria $k \leq$0.62 W/(m-K) it has an average outlet temperature of 275.03 K, and the design found using the velocity interpolation formulation has a considerable reduction in thermal resistance, though there is some perturbation in the conductivity of the solid. Additionally, ϕ_α of the optimized design is 1.84e-6.

5.3 Conclusions

The above numerical example demonstrates that defining conductivity in terms of the velocity field enables the optimization model to implicitly penalize porous flow to reduce thermal resistance. Moreover, the use of the Heaviside function helps define the conductivity of fluid regions accurately. The velocity interpolation model is extended to a 3d design case in the next chapter to minimize the thermal resistance of a heat exchanger.

The new model also provides an approach where the weights on the multi-objective function need not be tuned to meet performance requirements. The new model can independently optimize a design to either minimize thermal resistance or minimize viscous dissipation with an additional constraint function.

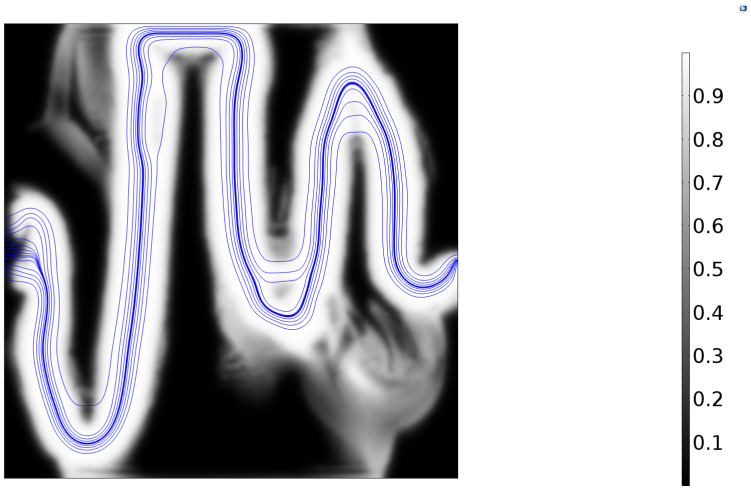

Figure 5.2: Density field (γ) and streamlines of the design optimized using the velocity interpolation formulation.

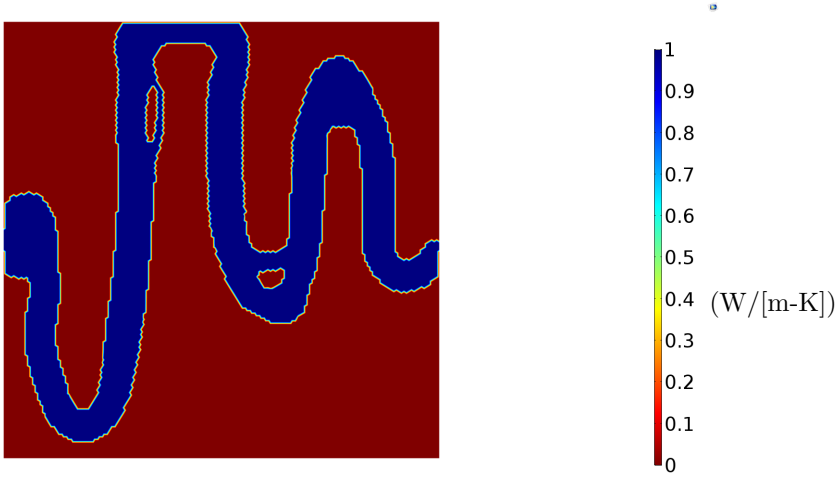

Figure 5.3: Conductivity distribution of the optimized design filtered with the criteria $k \leq 0.62$ W/([m-K]). The blue regions have conductivity below 0.62 W/([m-K]), and the plot shows the path taken by the fluid.

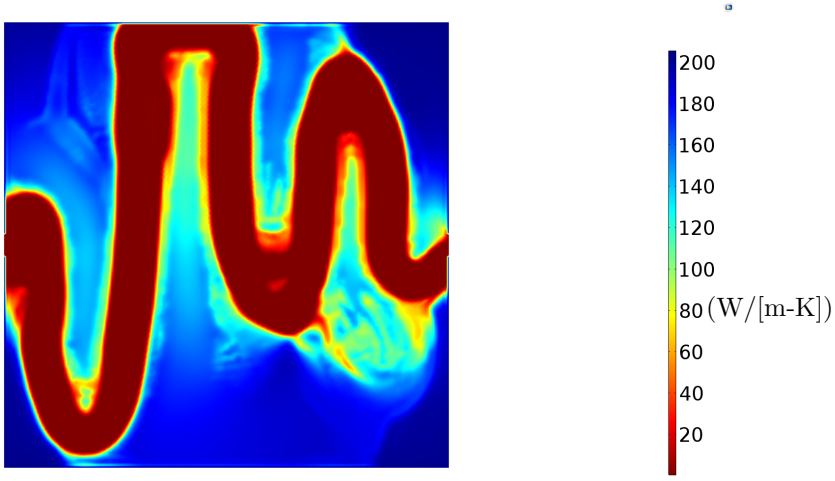

Figure 5.4: Conductivity distribution in the optimized design. The fluid channel increases area of contact with the metal by taking a meandering path to the outlet, which leads to an increase in heat transfer.

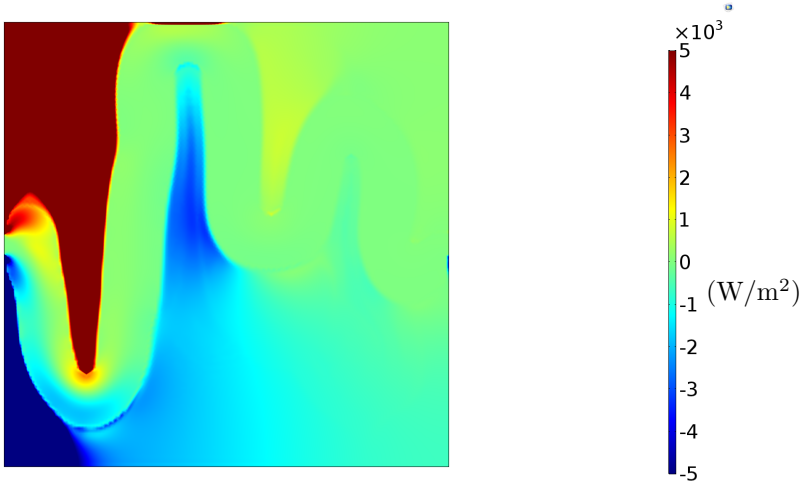

Figure 5.5: Vertical heat flux in the domain shows the heat lost by the fluid to the cold plates via the surrounding metal.

Chapter 6

Topology optimization of a 3d heat exchanger

In this chapter the velocity interpolation formulation implemented using the Heaviside function described in Chapter 5 is used in a 3d topology optimization design case. The goal of the optimization problem is to reduce the thermal resistance of the heat exchanger below that of the heat exchanger currently used in ASML. This is done to improve the speed of controlling the fluid outlet temperature with the Peltier elements working as actuators.

6.1 Reference design and definition of optimization problem

The fluid channel geometry of the reference heat exchanger design used at ASML is shown in Figure 6.1. The design has circular pipes surrounded by stainless steel. Hot fluid flows into the heat exchanger, and heat is removed from the fluid by Peltier elements to cool it. There are 4 Peltier elements placed on top of the stainless steel, and a constant temperature boundary condition is used to represent the Peltier elements in the steady state model. The boundary conditions of the design domain are given in Table 6.1, where T_{i} is the inlet temperature of the fluid and T_{c} is the temperature of each cold plate. The average outlet temperature of the fluid is 288.48 K in the reference design, while the viscous dissipation in it is 2.081e-6 W. The goal of the optimization problem is to find a heat exchanger design with a lower thermal resistance than the reference design while ensuring the viscous dissipation remains below that of the reference design.

Table 6.1: Boundary conditions of the heat exchanger.

Parameter	Magnitude
T_{i}	400 K
T_{c}	275 K
Inlet velocity	0.0129 m/s

6.2 Design domain of the optimization problem

Figure 6.2 illustrates the design domain of the optimization problem. The position of the inlet and outlet are shown with blue circles, and the grey region is the design space. The design requires the geometry of the fluid channel from inlet to outlet, with the metal the surrounding the fluid channels. Stainless steel is modeled with a conductivity of 14 W/(m-K). The Peltier elements are shown in green, and their positions are also given in Figure 6.2. Additionally, a Stokes flow model is used to find the velocity and pressure fields in the domain as the influence of the inertial terms on heat transfer are small in laminar flows.

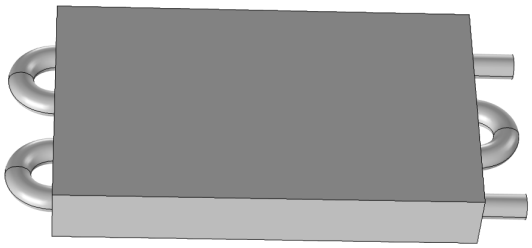

Figure 6.1: 3d model of the reference heat exchanger at ASML.

The optimization problem is formulated with the viscous dissipation of the reference design as a constraint, while the objective is to minimize the outlet temperature of the fluid. The optimization problem is defined as

$$\begin{aligned} \text{minimize} \quad & T_{\text{int}} \\ \text{subject to} \quad & \phi_{\text{d}}/(2.081e-6) \leq 1 \\ & 0 \leq \gamma_{\text{i}} \leq 1 \end{aligned}$$

The optimization routine is stopped if the outlet temperature of the fluid becomes equal to the temperature of the cold plates or if the change in outlet temperature becomes negligible with further model evaluations. Additionally, the parameters used in the optimization routine are given in Table 6.2.

Table 6.2: Parameters used in the velocity interpolation optimization model.

Parameter	Magnitude
$\boldsymbol{v}_{\max}$	0.0516 m/s
c_3	-26.8
c_4	27.4
t	300

6.3 Discussion of results

6.3.1 Evolution of the topology of the heat exchanger

The isosurface of $k = 0.62$ (W/m-K) is shown after a given number of iterations to study how the geometry of the fluid channel evolves to reduce the thermal resistance of the heat exchanger. Figure 6.3a shows the filtered geometry of fluid channel after 50 model evalutions. Initially the channels connecting the inlet and outlet are symmetric, and additional parallel channels direct the fluid from the inlet to the outet via the cold plates for heat transfer. After 100 model evaluations the fluid channel near the cold plates at the back end of the domain is formed, and this leads to a reduction in fluid outlet temperature from 298.41 K to 292.38 K. After 550 model evaluations an

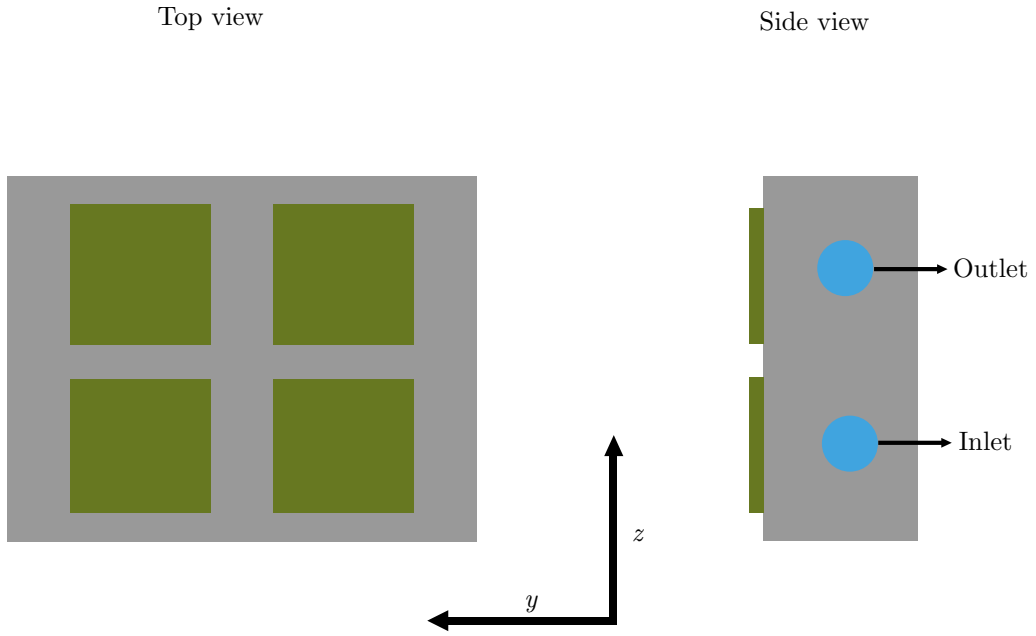

Figure 6.2: Design domain of the heat exchanger. The Peltier elements are shown in green and the blue circles indicate the inlet and outlet of the fluid.

additonal fluid channel is formed that directs fluid beyond the Peltier elements at the back, and this channel reduces the thermal resistance of the design by increasing the contact area between the fluid and the conductive solid via a long channel. The fluid channel near the inlet is directed further to the edges of the domain in this design to increase the length of this channel. Additionally, the first horizontal flow channel connecting the inlet and outlet has less fluid to increase the amount of fluid available in the outer fluid channels.

The average fluid outlet temperature and the viscous dissipation scaled with the viscous dissipation in the reference design are shown as function of model evaluations in Figures 6.4 and 6.5. The optimization routine is stopped as the change in outlet fluid temperature with model evaluations has become small. As the thermal resistance of the design is decreased by the optimization algorithm the viscous dissipation in the design increases as more fluid is directed through the longer channels in the domain.

Final design

The average fluid outlet temperature of the final topology optimized design is 275.98 K, while the ratio of the viscous dissipation of the design with respect to the viscous dissipation of the reference design is 0.0506. Figure 6.6 shows the temperature profile in the domain of the topology optimized design found using the porous flow model. The red regions in the figure show the hot fluid splitting into multiple channels. The solid is connected to the cold plate and it is relatively cool near the inlet when compared to the fluid. These solid regions conduct heat to the cold plates at the top. Figure 6.7 shows the velocity profile of the fluid in the design domain found using the porous flow model. The multiple fluid channels can be seen in this figure as well.

Figure 6.8 shows the density field of the topology optimized design. The post-processing criteria is however based on the conductivity distribution to filter the geometry of fluid channels with a large heat transfer coefficient. Figure 6.9 shows the isosurface of $k = 0.62$ W/(m-K). A strict post-processing criteria is used to capture the thickness of the fluid channels as thickness determines the heat transfer coefficient of a channel. There are only three parallel fluid channels in the final design, and the channel close to the inlet has been been nearly cut out. This reduces the thermal resistance of the design further. Moreover, the remaining parallel channels are essential as the amount of heat transferred depends on the temperature difference between the metal and fluid as well, and directing some fluid along the front and back cold plates is beneficial to reduce thermal

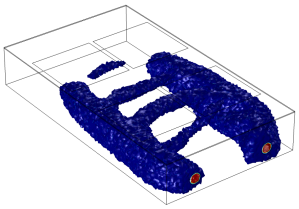

(a) The isosurface shows the fluid channel geometry after 50 model evaluations.

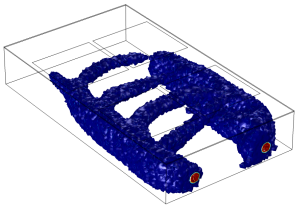

(b) The isosurface shows the fluid channel geometry after 100 model evaluations.

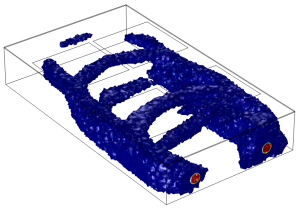

(c) The isosurface shows the fluid channel geometry after 200 model evaluations.

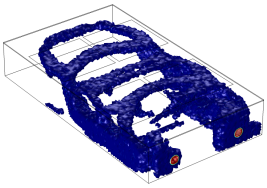

(d) The isosurface shows the fluid channel geometry after 550 model evaluations.

Figure 6.3: Isosurface of $k = 0.62$ (W/m-K) after a given number of model evalutions.

resistance. This is confirmed during post-processing by simulating a design with only the outer channel.

6.3.2 Post-processing to validate the optimization routine

The design is post-processed using the criteria $k \leq 0.62$ (W/m-K) to construct the fluid channel geometry (Figure 6.10). The coordinates of points in the domain that satisfy the filtering criteria are imported into SOLIDWORKS, and multiple sections of a channel are used to construct a continuous flow path. Channels are also connected where data points are missing to ensure fluid flows through the respective channel.

The post-processed design is simulated using the same boundary conditions and grid (2 mm tetrahedral elements linear in all fields) used in the optimization model to validate the design approach. Table 6.3 compares the performance of the reference design, the optimization model and the post-processed design. The results with a coarse grid indicate that the optimized result has a lower thermal resistance, while the viscous dissipation is also lower.

Table 6.3: Comparison of reference design, optimization model and post-processed design. The results are found using the grid used in the optimization model.

Design case	$\phi_{\mathrm{d,scaled}}$	T_{o}	R_{th}
Reference design	1	288.48 K	0.1764
Optimization model	0.0506	275.98	0.081
Post-processed design	0.526	277.89	0.1043

An additional simulation was performed with only the outer fluid channel (Figure 6.11) and the average fluid outlet temperature is 278.83 K, while the scaled viscous dissipation in it is 0.97239.

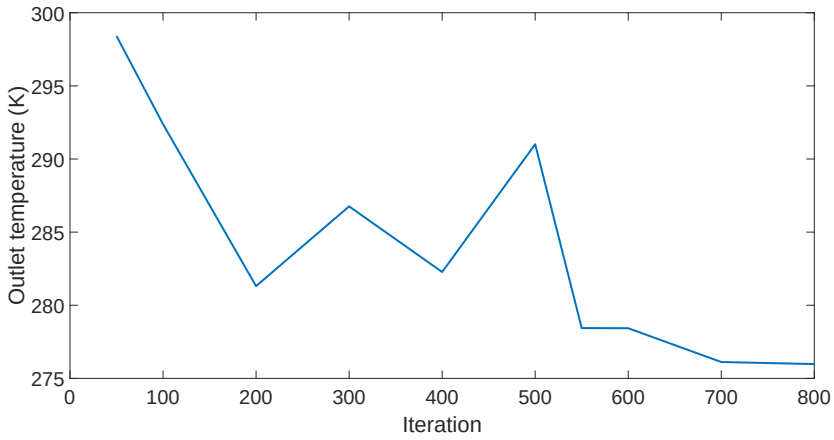

Figure 6.4: Average fluid outlet temperature as a function of model evalutions in the optimization routine.

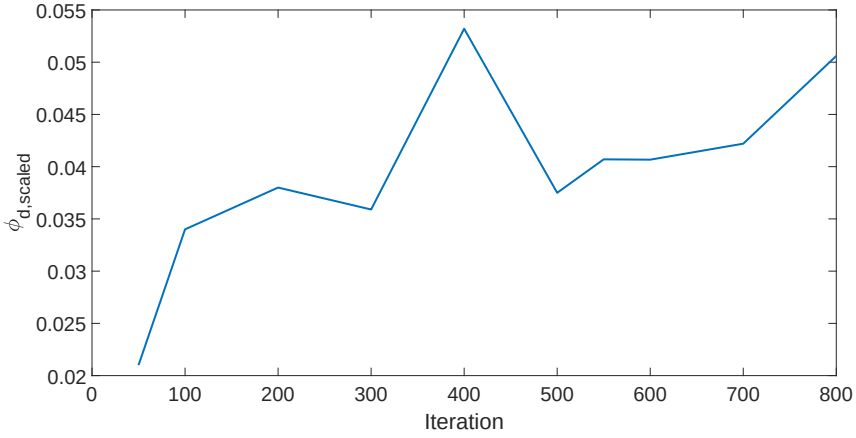

Figure 6.5: The viscous dissipation of the design scaled with the viscous dissipation of the reference design shown after a given number of model evalutions.

The average fluid temperature is slightly higher than in the topology optimized design, which shows that the parallel channels near the cold plates reduce thermal resistance. However, the viscous dissipation in the channel is much higher than in the topology optimized design as the distance travelled by the fluid channel is longer when compared to topology optimized design.

6.3.3 Viscous dissipation in the optimization model

The viscous dissipation in the post-processed design is much higher than the viscous dissipation in the optimization model. The optimization model has several additional parellal fluid channels whoose conductivity has not converged below 0.62. Figure 6.12 shows the isosurface of $k = 11$ (W/m-K). The red circles indicate the additional flow channels in the design. The lenient post-processing criteria can identify these additional channels, but the channel thickness is not modeled correctly. This leads to a higher thermal resistance of the post-processed design. Moreover these parallel channels reduce the amount of viscous dissipation in the design.

The viscous dissipation in a channel is inversely proportional to the Reynolds number for laminar flow in a channel with length L:

$$\Delta p = \frac{32\ \rho\ {v_\mathrm{m}}^2\ L}{Re\ d}. \tag{6.1}$$

However, the heat transfer coefficient of a channel is independent of the Reynolds number, which is why a design with multiple parallel channels is preferred in a laminar heat exchanger. The

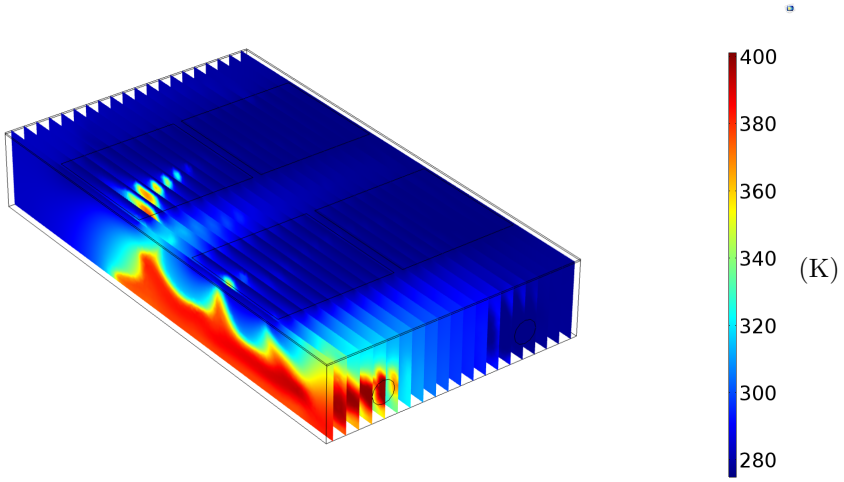

Figure 6.6: Temperature profile in the 3d topology optimized design.

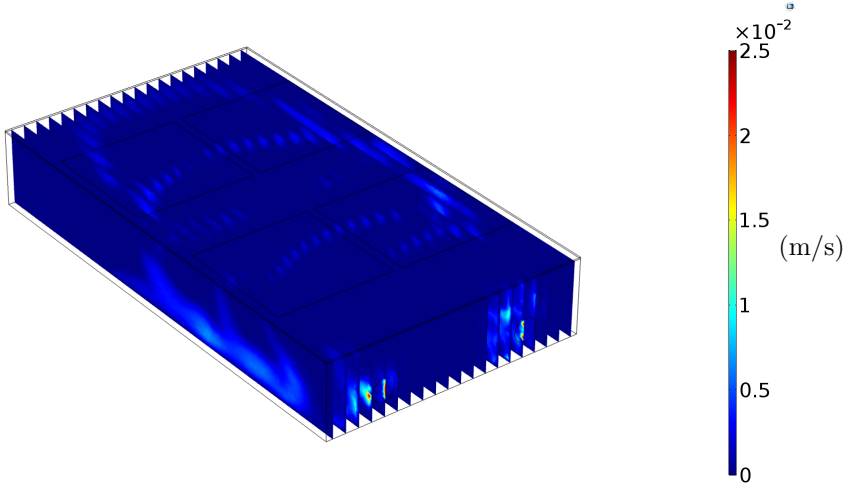

Figure 6.7: Velocity plot in the 3d topology optimized design.

topology optimization model has conductivity defined as a function of the velocity field, and the optimizer takes advantage of the model in this case by creating many low velocity fluid channels. This allows the optimizer to increase the diffusion coefficient in these fluid channel and increase the heat transferred from the fluid to the solid. The pressure drop in these channels is also small as it scales inversely with Reynolds number. Either a steeper approximation of the Heavisde function is required or another strategy needs to be developed to overcome this drawback in the optimization model.

6.3.4 Grid independent results

A grid independent result is defined as a one that has negligible numerical change when the element size in the finite element model is reduced. The performance parameters of the final design is compared with that of the reference design using the grid independant results in Table 6.4. The topology optimized design has narrow horizontal channels that are not well resolved with a coarse mesh, and the amount of viscous dissipation is underestimated in these regions. The final design has a 14.14 % decrease in thermal resistance, while the viscous dissipation is 5.3% lower than in the reference design.

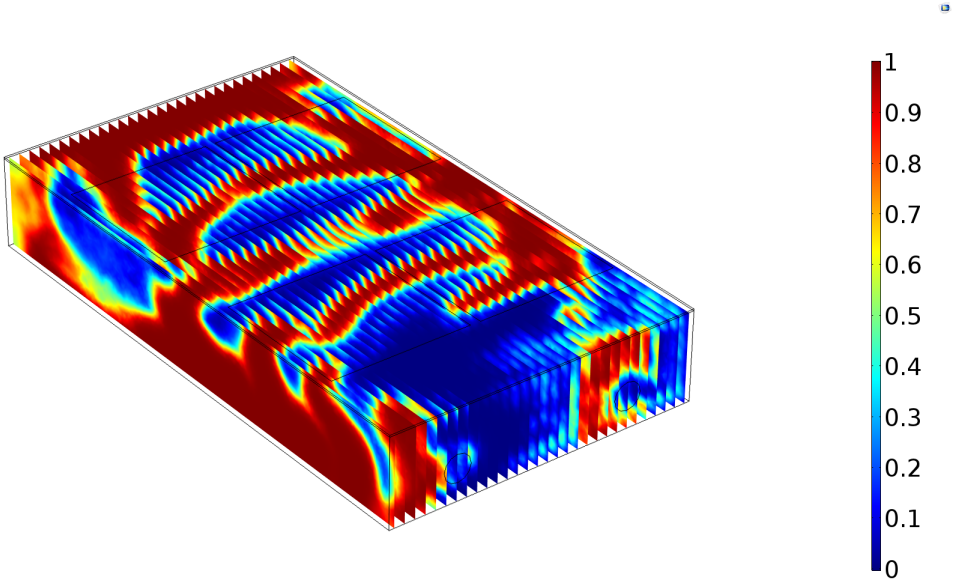

Figure 6.8: Density field (γ) of the 3d optimized design.

Table 6.4: Comparison of reference design and the post-processed design using grid independent results.

Design case	ϕ_{d}	T_{o}	R_{th}
Reference design	3.08e-6	309.7 K	0.3066
Post-processed design	2.917e-6	303.097 K	0.2633

6.4 Conclusions

The viscous dissipation in the optimization model is much lower than in the the post-processed design as many fluid channels are filtered to find a design with a low thermal resistance. A strategy to prevent the diffusion coefficient of the fluid from changing from its setpoint needs to be developed in order to match the thermal resistance and viscous dissipation of the optimization model and the post-processed design.

Moreover, the grid independent results show a large deviation from the results with the coarse grid in the optimization model. A finer grid is necessary in the optimization model to find a better estimate of the performance parameters during the optimization routine.

The final results demonstrate that the velocity interpolation model is capable of finding designs with high heat transfer coefficients, and reduce the thermal resistance of heat exchanger designs. The thermal resistance of the topology optimized design is 14.14 % lower than the thermal resistance of the reference design at ASML, and the viscous dissipation is 5.3% lower in the topology optimized than in the reference design.

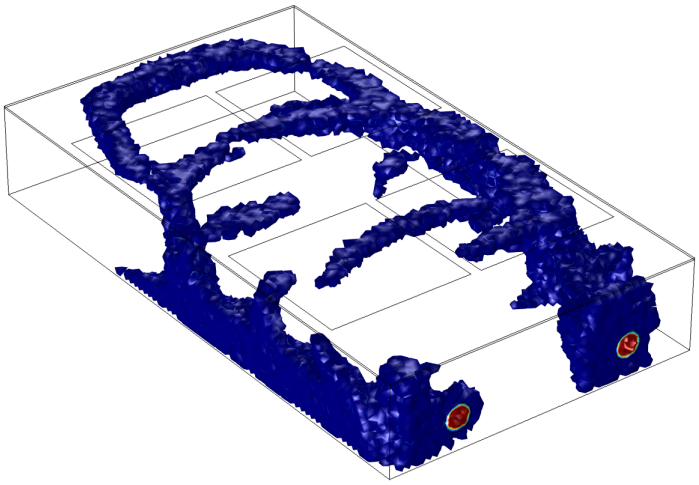

Figure 6.9: Isosurface of $k = 0.62$ (W/m-k). The isosurface shows the fluid channel geometry after 850 model evaluations.

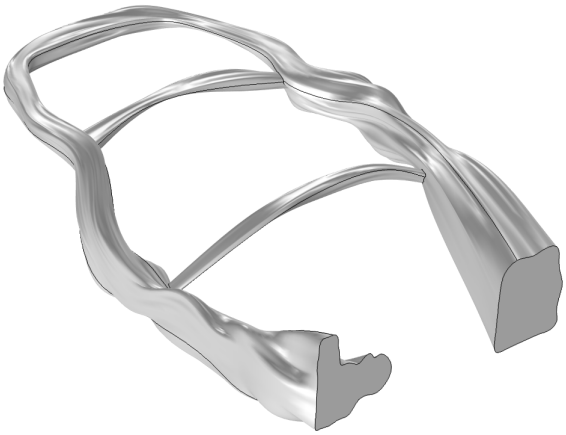

Figure 6.10: Toplogy optimized design post-processed using the criteria $k \leq 0.62$ (W/m-K).

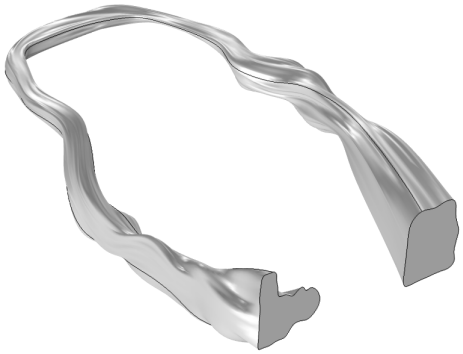

Figure 6.11: Geometry of the outer fluid channel of the topology optimized design.

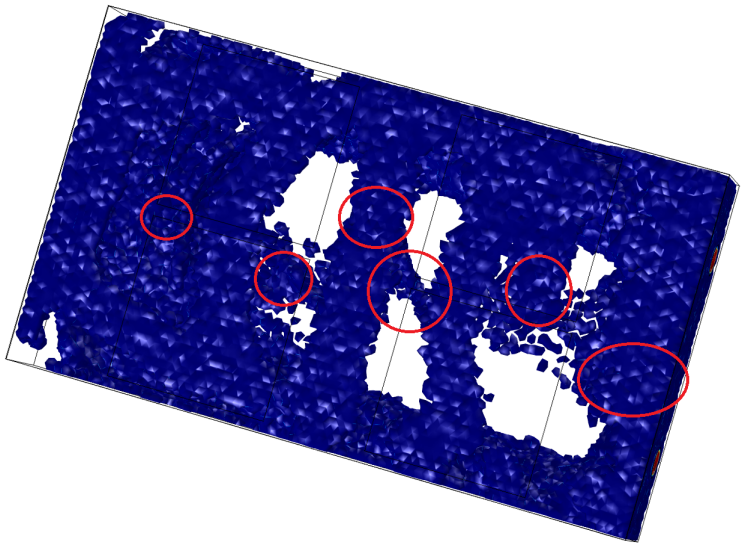

Figure 6.12: Isosurface of $k = 11$ (W/m-K). The isosurface shows the fluid channel geometry with a lenient post-processing criteria. The red circles indicate the additional flow channels.

Chapter 7

Conclusions and recommendations

7.1 Conclusions

The goal of this study was to implement a topology optimization method to decrease the thermal resistance of a heat exchanger, while still controlling the amount of viscous dissipation in the design. Heat exchangers generally have a metal with a larger conductivity than the fluid used in the heat exchanger. Peltier elements are placed on the conductive solid to remove heat from the fluid in the heat exchanger at ASML. The Peltier elements are used to control the outlet temperature of the fluid for conditioning machine components. Reducing the thermal resistance of the heat exchanger enables faster control of the fluid outlet temperature.

The heat exchanger was designed using topology optimization in this study. The use of topology optimization for the design of heat exchangers requires the finite element model for fluid flow and heat transfer. The respective finite element models are then combined with a continuous design optimization variable that is allocated to each element in the design domain. This allows complex free form structures to evlolve during the optimization routine.

Chapter 3 implements a topology optimization model where emphasis was placed on convective heat transfer. A uniform conductivity was allocated to all regions in the domain. A multi-objective function with one function reducing thermal resistance and another reducing viscous dissipation was used in this chapter. The results provided an intuition on the mechanisms to increase convection heat transfer in low Reynolds number flows.

In Chapter 4 the density based interpolation scheme (density is design variable in this instance) of allocating conductivity in the design domain found in literature was tested. The designs found using this scheme were promising when the goal of the optimization problem was to minimize viscous dissipation. However, the density based interpolation of conductivity did not produce designs that with the desired reduction in thermal resistance. Since a porous flow model is used in the optimization scheme, flow through porous regions need to be explicitly penalized in the density based conductivity interpolation scheme to obtain feasible designs. The erosion in the optimization model is demonstrated with a numerical example when a single objective function of minimizing the thermal resistance is used. The optimizer takes advantage of the porous flow model and produces designs with large porous flow and large conductivity. This shows a large numerical reduction in thermal resistance as convection is modeled with the conductivity of the solid.

A new conductivity interpolation scheme was proposed with the conductivity allocated as a function of the velocity field in Chapter 5. Designs with a clear sepation of solid and fluid were found without explicitly penalizing porous flow with this model. A clear separation of solid and fluid materials reduces the thermal resistance of the design with the solid conducting heat and the fluid convecting it. Additionally, the thermal resistance of the numerical example in this chapter showed a significant reduction when compared to the results of density based conductivity interpolation model.

Chaper 6 implements the velocity based conductivity interpolation scheme in a 3d optimization model. The goal of the 3d optimization routine is to minimize the thermal resistance of the design

while maintaining the viscous dissipation in the design below that of the baseline heat exchanger design at ASML. The results of the optimization routine indicated a significant reduction in thermal resistance and viscous dissipation. The topology optimized design had several low velocity parallel fluid channels, and these channels had a higher diffusion coefficient than the setpoint defined for the diffusion coefficient of the fluid. This resulted in a design that had low viscous dissipation, while the indicated thermal resistance was low as well. However, the viscous dissipation in the post-processed topology optimized design was higher than in the optimization model as several fluid channels were removed using a strict conductivity based post-processing criterion. A strict post-processing criterion is implemented to find the geometry of regions that contribute to a large reduction in thermal resistance.

Moreover, a strategy to prevent the diffusion coefficient of the fluid from changing significantly is necessary to ensure that the results of the optimization routine match with the results of the post-processed design. Finally, the topology optimized design was compared to the baseline heat exchanger design at ASML using grid independent results. The results showed a large change from the coarse grid used in the optimization routine, and this indicates that a finer grid is necessary to find a better estimate of the performance parameters in the optimization model. The topology optimized design has a 14.14 % reduction in thermal resistance and a 5.3% reduction in viscous dissipation when compared to the baseline design at ASML.

7.2 Recommendations

The velocity interpolation formulation has the tendency to form multiple parallel channels as this can increase the diffusion coefficient in these channels if the velocity of the fluid is low. Moreover, using a strict post-processing criteria results in a post-processed design with a different viscous dissipation when compared to the viscous dissipation in the optimization model. Either a steeper conductivity interpolation scheme needs to be tested or another method is necessary to ensure the conductivities of the fluid channels converge close to the conductivity of the fluid.

The final design goal of the active heat exchanger system is to suppress temperature fluctuations of the supply fluid. This requires a transient study. The thermal damping of the metal will also influence the optimal material distribution in the domain when a transient study is used. The current topology optimization model should be extended to a transient setting to further optimize the design.

Finally, the optimization routine can be extended to optimize design cases with a larger Reynolds number. A change in Reynolds number affects the mass flow distribution, pressure drop, and the heat transfer behaviour. This extension requires the use of finer meshes, hence more computing time, and further studies on the solvers used with the optimization model.

Bibliography

[1] Thomas Borrvall and Joakim Petersson. Topology optimization of fluids in stokes flow. International journal for numerical methods in fluids, 41(1):77–107, 2003.

[2] M Pietropaoli, R Ahlfeld, F Montomoli, A Ciani, and M D'Ercole. Design for additive manufacturing: Internal channel optimization. Journal of Engineering for Gas Turbines and Power, 139(10):102101, 2017.

[3] Christian J.L. Hermes and Jader R. Barbosa Jr. Thermodynamic comparison of peltier, stirling, and vapor compression portable coolers. Applied Energy, 91(1):51 – 58, 2012.

[4] David Michael Rowe. CRC handbook of thermoelectrics. CRC press, 1995.

[5] Frank M White and Isla Corfield. Viscous fluid flow, volume 3. McGraw-Hill Higher Education Boston, 2006.

[6] Stephen Boyd and Lieven Vandenberghe. Convex optimization. Cambridge university press, 2004.

[7] Martin P Bendsøe, Ole Sigmund, Martin P Bendsøe, and Ole Sigmund. Topology optimization by distribution of isotropic material. Springer, 2004.

[8] VK Patel and RV Rao. Design optimization of shell-and-tube heat exchanger using particle swarm optimization technique. Applied Thermal Engineering, 30(11):1417–1425, 2010.

[9] Kwasi Foli, Tatsuya Okabe, Markus Olhofer, Yaochu Jin, and Bernhard Sendhoff. Optimization of micro heat exchanger: Cfd, analytical approach and multi-objective evolutionary algorithms. International Journal of Heat and Mass Transfer, 49(5):1090–1099, 2006.

[10] Renan Hilbert, Gábor Janiga, Romain Baron, and Dominique Thévenin. Multi-objective shape optimization of a heat exchanger using parallel genetic algorithms. International Journal of Heat and Mass Transfer, 49(15):2567–2577, 2006.

[11] A. Gersborg-Hansen, O. Sigmund, and R.B. Haber. Topology optimization of channel flow problems. Structural and Multidisciplinary Optimization, 30(3):181–192, 2005.

[12] Sebastian Kreissl and Kurt Maute. Levelset based fluid topology optimization using the extended finite element method. Structural and Multidisciplinary Optimization, 46(3):311–326, 2012.

[13] Allan Gersborg-Hansen, Martin P Bendsøe, and Ole Sigmund. Topology optimization of heat conduction problems using the finite volume method. Structural and multidisciplinary optimization, 31(4):251–259, 2006.

[14] Gilles Marck, Maroun Nemer, Jean-Luc Harion, Serge Russeil, and Daniel Bougeard. Topology optimization using the simp method for multiobjective conductive problems. Numerical Heat Transfer, Part B: Fundamentals, 61(6):439–470, 2012.

[15] T Gao, WH Zhang, JH Zhu, YJ Xu, and DH Bassir. Topology optimization of heat conduction problem involving design-dependent heat load effect. Finite Elements in Analysis and Design, 44(14):805–813, 2008.

[16] Gilles Marck, Maroun Nemer, and Jean-Luc Harion. Topology optimization of heat and mass transfer problems: Laminar flow. Numerical Heat Transfer, Part B: Fundamentals, 63(6):508–539, 2013.

[17] Adriano A Koga, Edson Comini C Lopes, Helcio F Villa Nova, Cícero R de Lima, and Emílio Carlos Nelli Silva. Development of heat sink device by using topology optimization. International Journal of Heat and Mass Transfer, 64:759–772, 2013.

[18] Ercan M Dede. Multiphysics topology optimization of heat transfer and fluid flow systems. In proceedings of the COMSOL Users Conference, 2009.

[19] Kyungjun Lee. Topology Optimization of convective Cooling System Designs. PhD thesis, University of Michigan, 2012.

[20] Krister Svanberg. Mma and gcmma, versions september 2007. Optimization and Systems Theory, page 104, 2007.

[21] Boyan Stefanov Lazarov and Ole Sigmund. Filters in topology optimization based on helmholtz-type differential equations. International Journal for Numerical Methods in Engineering, 86(6):765–781, 2011.

[22] Theodore L Bergman and Frank P Incropera. Fundamentals of heat and mass transfer. John Wiley & Sons, 2011.

[23] Kays W.M. Trans. ASME, 77(1265), 1955.

Appendix A

Steady state energy balance in Peltier elements

This appendix explains the steady state equations that set the cold and hot plate temperatures of the Peltier element for a given fluid channel geometry at the supply and dump side. The Peltier element is current controlled. When a current runs through the p-n junction a temperature difference develops across the conductors because of the Peltier effect. The relationship between current and temperature difference is found using the following equation [4]

$$I = \frac{S\Delta T}{R[(1 + ZT_{\mathrm{m}})^{1/2} - 1]}, \tag{A.1}$$

where Z is the thermoelectric figure of merit of a material and T_{m} is the mean temperature of the Peltier.

Additionally the heat removed from the cold plate of the Peltier element is

$$Q_{\mathrm{c}} = SIT_{\mathrm{c}} - K\Delta T - I^2R/2, \tag{A.2}$$

and the heat added to the hot plate of the Peltier element is

$$Q_{\mathrm{h}} = SIT_{\mathrm{h}} + K\Delta T + I^2R/2. \tag{A.3}$$

Q_{c} and Q_{h} depend on the fluid channel geometries as explained in Chapter 1. The first term on the right hand side of Equations A.2 and A.3 is heat carried by the majority charge carries of the conductor, the second term is back conduction of heat from the hot plate to the cold plate and the third term is the heat dissipated because of Joule heating. Equations A.1, A.2 and A.3 are used to find ΔT, T_{c} and T_{h} for a given current.

Moreover, the Peltier element also has a point of stability when Q_{c}=0 beyond which additional cooling is not possible with an increase in current, and the nonlinear relationship between the current and heat transferred determines the optimal operating range of the Peltier element.

Appendix B

Thermal resistance of internal flows

Thermal resistance is defined as the ratio of the temperature difference to the amount of heat transferred. Consider the internal flow shown in Figure B.1 where the fluid enters the duct with a mean inlet temperature $T_{\mathrm{m,i}}$, flows along a plate at a temperature T_{s} and exits with a mean outlet temperature $T_{\mathrm{m,o}}$. The average heat transfer coefficient of the duct is defined in terms of the logarithmic mean temperature difference

$$\Delta T_{\mathrm{lm}} = \frac{\Delta T_{\mathrm{o}} - \Delta T_{\mathrm{i}}}{\ln(\Delta T_{\mathrm{o}}/\Delta T_{\mathrm{i}})}, \tag{B.1}$$

where $\Delta T_{\mathrm{i}} = T_{\mathrm{s}} - T_{\mathrm{m,i}}$ and $\Delta T_{\mathrm{o}} = T_{\mathrm{s}} - T_{\mathrm{m,o}}$. The heat transferred via convection is

$$q_{\mathrm{conv}} = \overline{h} A \Delta T_{\mathrm{lm}}, \tag{B.2}$$

where $\bar{h}$ is the average heat transfer coefficient of the duct. Therefore the thermal resistance for an internal flow is

$$R_{\mathrm{th}} = \frac{\Delta T_{\mathrm{lm}}}{q_{\mathrm{conv}}}. \tag{B.3}$$

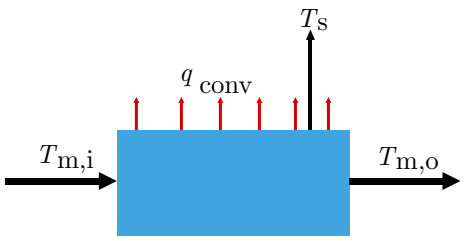

Figure B.1: Internal flow through a duct with a temperature boundary condition.

Appendix C

Influence of channel geometry on heat transfer

This appendix explains the influence of channel geometry on heat transfer coefficient for laminar flow through ducts. As the fluid flows against a plate with a constant temperature it loses or gains heat depending on its average temperature, and the amount of heat transferred depends on the temperature difference between them and the heat transfer coefficient. The total amount of heat transferred from or to the fluid in internal flows is found using [22]

$$\dot{m}C_p\Delta T = \bar{h}A\Delta T_{\mathrm{lm}}, \tag{C.1}$$

where $\dot{m}$ is the mass flow rate of the fluid. Additionally the local heat transfer coefficient is defined as

$$h = \frac{k\frac{dT}{dy}|_{wall}}{T_{\mathrm{s}} - T_{\mathrm{avg}}}, \tag{C.2}$$

where the temperature gradient at the wall ($\frac{dT}{dy}|_{wall}$) defines the heat transferred between the plate and the fluid, T_{s} denotes the temperature of the plate and T_{avg} is average temperature of the fluid in the channel. The local heat transfer coefficient is a function of the fluid channel geometry. For a fully developed laminar flow in a circular tube the local heat transfer coefficient is

$$h = \frac{3.66k}{d}, \tag{C.3}$$

where d is the channel diameter. The heat transfer coefficient is independant of the Reynolds number, and it is directly proportional to the channel diameter. The flow is fully developed when the velocity profile, and the non-dimensional temperature field remain constant in the flow direction.

At the entrance region the temperature profile of the fluid is uniform and the heat transfer coefficient is larger here. The average temperature is the same as the fluid temperature at the wall, therefore the heat flux for a given difference between T_{s} and T_{avg} is higher. The correlation for the average heat transfer coefficient in the entrance region is [23]

$$\frac{hd}{k} = 3.66 + \frac{0.0668(d/x)RePr}{1 + 0.04[(d/x)RePr]^{2/3}}, \tag{C.4}$$

where Pr is the Prandtl number of the fluid. The Prandtl number of water is 7.2. The thermal entrance length of an 8mm tube with water flowing at a Reynolds number of 1 is 4.5mm. The 2d design domain has a length of 140mm, and the temperature profile of the fluid settles down in a short distance for low Reynolds numbers.

An additional mechanism to increase the heat transfer coefficient in laminar flows is to generate secondary flow with the help of helical coils as shown in Figure C.1. The secondary flow carries heat from the wall and with the help of mixing, to maintain the average fluid temperature close to the fluid temperature at the wall, it maintains a high heat transfer coefficient in the channel.

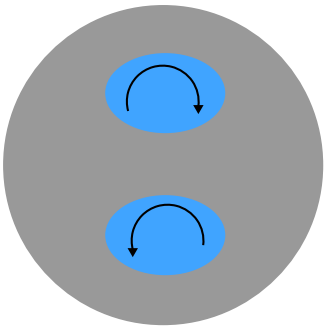

Figure C.1: Secondary flow induced by helical coils to enhance heat transfer, with flow in the axial direction.